EasyChair Preprint

№ 5433

Mechanisms of Self-Ordering in the Synthesis of Quasi-One-Dimensional Periodic Core-Shell Nanostructures

Vyacheslav Gorshkov and Vladimir Tereshchuk

April 30, 2021

Mechanisms of self-ordering in the synthesis of quasi-one-dimensional periodic core-shell nanostructures

Vyacheslav N. Gorshkov[1,2], Vladimir V. Tereshchuk[1]

[1] National Technical University of Ukraine, Igor Sikorsky Kyiv Polytechnic Institute, 37 Prospect Peremogy, Kiev 03056, Ukraine

[2] Center for Advanced Materials Processing, Departments of Chemistry and Physics, Clarkson University, Potsdam, New York 13699, United States

Corresponding author. Email: v.gorshkov@kpi.ua

Keywords: Diameter-modulated nanowire, nanoclusters, surface morphology, core/shell synthesis, homoepitaxial growth

Abstract

We have analyzed the physical mechanisms responsible for the formation of an ordered sequence of nanoclusters synthesized on a nanowire in the diffusion mode of deposition of free atoms. The results were obtained using a kinetic Monte Carlo Model, which takes into account only the interaction between the nearest atoms of the crystal lattice. Nevertheless, this model describes the correlations between the elements of the system at distances significantly exceeding their sizes. We show that the long-range spatial correlation between the synthesized clusters is due to two factors; first, the surface diffusion in the metastable system of deposited atoms which leads to the formation of primary nuclei, and second, the shadow effect arising when growing nanoclusters become rather large. It is these processes that are the "tools" through which individual clusters suppress the development of their neighboring nuclei in the competition for survival and form high self-ordering at the final stage of synthesis. Numerical experiments were carried out for one-dimensional systems with a diamond-like lattice structure. The features of manifestation of self-ordering effects are investigated in detail depending on the orientation of the basic nanowire, temperature, and the rate of supply of free atoms into the system. The observed variety of morphologies of one-dimensional systems at the final stage of synthesis is in good agreement with numerous experimental data obtained during the synthesis of nanoclusters on silicon and germanium nanowires. On the basis of the obtained results, optimal synthesis modes are proposed for increasing the regularity in the localization of synthesized nanoclusters.

1. Introduction

Nowadays, semiconductor nanowires are the subject of extensive studies because their favorable properties make them promising candidates for various engineering applications. Specifically,

high electrical and low thermal conductivity **[1,2]**, field emission **[3-5]**, and quantum confinement effects **[6]** make silicon nanowires potentially useful as building blocks for thermoelectric and photonic devices like nanowire field-effect transistors **[7-9]**, ultra-sensitive biological, chemical or mass sensors **[10-19]**, and photodetectors **[20-22]**. Moreover, nanowires produced via metal-assisted chemical etching (MACE) **[23,24]** possess strong broadband optical absorption and low reflectance which make them particularly interesting for the new generation of solar cells **[25-38]**. New functionalities as well as the enhancement of existing physical properties, such as thermal transport and optical absorption of nanowires, can be introduced by tuning their composition and morphology **[39-49]**. For example, thanks to their large stretchability, silicon nanowire springs **[50]** are now used for the fabrication of sensitive biosensors **[50]** and core-multi-shell semiconductor nanowires (CMS) with embedded quantum dots **[51,52]** can be exploited in the manufacturing of solid-state lighting devices. In a recent study **[53]**, an innovative approach of synthesis of spring-like structures, which may serve as vibrant resonators on bamboo-shaped Si- nanowires, was introduced. However, it should be noted that the synthesis of nanowires with desirable morphological features, such as high periodicity of diameter modulated core/shell nanowire heterostructures, remains a scientific challenge. The solution to this problem requires a better understanding of the role of various factors as well as physical mechanisms in process dynamics and their influence on the self-organization of the structures that cover the nanowire core.

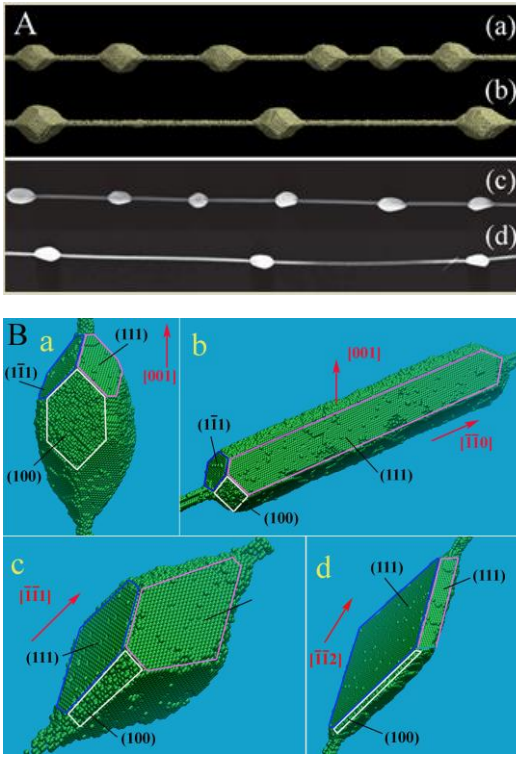

Figure 1. Diffusive growth of periodic shells on nanowires with the diamond cubic crystal structure. (A) Configurations (a) and (b) present the results of our Monte-Carlo model obtained for different external fluxes of free atoms, $\Gamma_{surf}^{(+)}$, to the nanowire surface: $\Gamma_{surf}^{(+)}(a) > \Gamma_{surf}^{(+)}(b)$. Configurations (c) and (d) show the experimental results [38] obtained in similar conditions on depositing Ge-atoms onto Si-nanowire cores at 520°C. (B) Various shapes of synthesized nanoclusters formed on nanowires with different orientations, resulted from our numerical experimentations.

In this work, we reveal the mechanisms of self-organization in the synthesis of a system of nanoclusters formed by the deposition of germanium or silicon atoms onto nanowires of the same materials. The choice of such a subject to study is beneficial because the conclusions of our theoretical work can be compared with the numerous results of experiments [38] carried out in the physical systems, the dynamics of which is expressly anisotropic, i.e. depends on the orientation of the basic nanowire axis relative to its internal crystal structure (see Fig. 1B), so that the claimed theoretical statements can be extensively verified. This anisotropy manifests itself both in the shape of clusters formed and in

the mechanism of self-ordering of their nuclei, which can be caused by completely different factors, as shown in our work. The diversity of these factors we demonstrate below with a couple of results obtained in [38].

The synthesis of Si-nanoclusters **[38]** occurs at a rather high temperature ($T{\sim}750^{o}-900^{o}\mathrm{C}$). At such temperature regimes and in the absence of an external flux of free atoms to the surface of the nanowire, the nanowire can decompose into separate nanodroplets as a result of thermal instability with respect to the periodic perturbations of its cross-section [**38, 54-56**]. However, the external diffusion flux of atoms may suppress this instability (preventing the nanowire break-up into a chain of nanodroplets) and form a one-dimensional core-shell structure with periodic short-wave radius modulations **[38]**. Naturally, that in this case, it is the tendency to the spontaneous excitation of periodic surface perturbations (with wavelength $\lambda \approx (4.5-5.5)r_0$ in some nanowire orientations [54]) that can impose the corresponding length of synthesized clusters in relation to the average diameter of a one-dimensional system due to the concentration of diffusion fluxes of free atoms into the regions of emerging broadenings (zones of greater surface curvature, which become as seeds of heterogeneous nucleation). Moreover, this initiated redistribution of space diffusive fluxes increases the surface diffusion of deposited atoms from broad to narrow regions that prevents the disintegration of the growing structure.

However, the periodicity, Λ, of the emerging nanoclusters can significantly exceed (see Fig. 1A) the value r_0 ($\Lambda/r_0 \gtrsim 60$-see Fig. 1A(d)) which cannot be associated with the manifestation of thermal instability of the nanowire surface. At a temperature of $\sim 550^{o}\mathrm{C}$, the synthesis time of newly formed nanoclusters is much shorter than the break-up time of the basic silicon nanowire, which is equal to several tens of hours **[38]**. Thus, the interpretation of the formation of a periodic chain of "nanodroplets" of deposited Ge-atoms as a manifestation of the Rayleigh-Plateau-like instability **[38]** in the subsystem of surface germanium atoms is unconvincing at the observed "giant" values of the parameter Λ/r_0 (Fig. 1A(d); (the value of the parameter Λ/r_0, predicted by the Rayleigh-Plateau theory, is around 9). It should be noted that even in the Si-Si core-shell synthesis these giant Λ/r_0 values (up to $\Lambda/r_0 \gtrsim 80$) are observed [**38**] for some nanowire orientations when the thermal instability is impeded [**54**].

The results of our numerical experiments, obtained on the basis of the mesoscopic kinetic Monte Carlo model (presented in Section II), demonstrate general conceptions about the driving physical mechanisms of the observed self-ordering (see Sections III). In the most common cases, when thermal instability is not a determining factor in the dynamics of the system, in a brief, rough summary, they can be described as follows.

Atoms deposited onto the nanowire with a flux density $\Gamma_{surf}^{(+)}$ form a "gas" diffusing over the nanowire surface. This surface presents a quasi-one-dimensional space for the gas to chaotically move.

With a sufficient flux density, $\Gamma_{surf}^{(+)}$, the surface gas density, n_s, determined by the balance between $\Gamma_{surf}^{(+)}$ and the sublimation flux density $\Gamma_{subl}^{(-)}$, increases to the critical level, $n_s^{(cr)}$, sufficient for the formation of a metastable gas state. Further dynamics of the system basically

corresponds to the Gibbs' theory of homogenous nucleation **[57, 58]**. The nuclei of a new phase fluctuationally formed from the deposited atoms arise with the size above critical (the subsequent disintegration of such clusters into fragments becomes unlikely). These nuclei, absorbing surrounding deposited atoms, create zones of low density to the left and right of themselves, in which $n_s < n_s^{(cr)}$ and therefore the formation of new nuclei is impeded. It is the size of these zones, $\mathcal{L}_{diff}$, that determines the self-ordering parameter, Λ. In turn, the $\mathcal{L}_{diff}$ value depends on the parameters monitored in the experiments – the temperature and $\Gamma_{surf}^{(+)}$ (see Fig. 1A, configurations (a) and (b), and (c) and (d)). The minimization of the free energy of slowly-growing single nanoclusters during synthesis leads to significant differences in their shapes (Fig. 1B) depending on the nanowire orientation. Note that the growth of the formed nanoclusters in height redistributes the space diffusion fluxes ($\Gamma_{surf}^{(+)}$, respectively) along the nanowire and introduces additional factors to the mechanisms of self-organization of the chain of nanoclusters.

2. Model

In the current work, we use the kinetic Monte Carlo (MC) approach which was previously successfully applied to study the growth and sintering of nanoparticles **[59-63]**, formation of nanoclusters and nanopillars in non-equilibrium surface growth **[64-65]**, and the break-up of nanowires with the FCC, BCC, and diamond-like lattice structures into isomeric nanoparticles **[66-69]**. The description of the model can be found in the aforementioned studies. Here we detail some concepts and attributes of this model used in the problem under consideration.

The computational domain/container is a cylinder with a length, L, and a radius, R, that encloses a nanowire of radius r_0 located along its axis ($R \gg r_0$). The growth of nanoclusters on the nanowire, which has the diamond cubic crystal structure, is determined by the diffusion fluxes of free atoms from the surrounding space to the nanowire surface at a given concentration, n_{free}, of these atoms near the side wall of the cylinder. Free atoms hop in random directions with a fixed-length step, ℓ, and are reflected by the boundary of the container. They can attach to the surface of the nanowire at vacant sites that are contiguous to the sites occupied by the nanowire atoms. Each site represents a region in space delineated by the Wigner-Seitz unit-lattice cell. If one of the atoms hops into such a cell, it becomes attached to the nanowire and located at the center of the corresponding Wigner-Seitz cell. It should be noted that the hopping attempt is blocked when the atoms try to hop into the occupied lattice sites. When an atom is attached, it can either move on the surface of the nanostructure (the rules of surface dynamics will be addressed shortly) or detach from it and become free again.

We represent the dynamics of the nanosystem in the form of sequential frames of a "cartoon". For a detailed description of the process, the time interval between two consecutive frames, Δt, should be chosen such that each atom makes no more than one jump during this time. Free atoms are the most mobile, therefore the logical choice of the unit of time in our model is the scattering time of these atoms, τ, i.e. $\Delta t/\tau = 1$. The frequency of jumps of bound surface atoms to the

nearest vacancies of the crystal lattice, ν, is lower than $1/\Delta t$, $\nu < 1/\Delta t$. In dimensionless units $\nu < 1$, or $P < 1$, where P $(P = \nu)$ is the jump probability, which, moreover, is rather inhomogeneous on the nanostructure surface. Therefore, per unit time, we randomly scan over the entire system of free and bound atoms and determine for the selected atoms the result of two successive random events - (i) whether the atom will jump and (ii) to which of the nearest vacancies it will move if the jump occurs. We define this calculating procedure of the next frame of system evolution as one Monte Carlo (MC) step. Thus, *on average*, each free atom hops once per unit of time, whereas lattice atoms have *only one hopping attempt* on average.

2.1 Basic probabilistic relations. The atoms attached to the nanostructure can hop to the nearest-neighbor vacant lattice sites. If an atom has m_0 nearest neighbors ($m_0 < m_c$; m_c= 4 is the coordination number for the diamond cubic lattice), it is assumed that the hopping probability for this atom is p^{m_0}, where $p = e^{-\Delta/kT} < 1$, and $m_0\Delta > 0$ is the activation free-energy barrier. If the hopping takes place, the atom either ends up in one of its $m_c - m_0$ vacant nearest neighbor sites, or returns to its original site. The probability, $p_{target}^{(i)}$, of each of the $(m_c - m_0 + 1)$ possible target sites $(i = 0, 1, \dots, m_c - m_0)$ is proportional to the corresponding Boltzmann factor, $\sim\exp(m_t^{(i)}|\varepsilon|/kT)$, with $\varepsilon < 0$ measuring the free-energy of the binding at the target sites, and $m_t^{(i)}$ is the number of nearest neighbors in the prospective new state. Note that index $i = 0$ corresponds to the initial state with $m_t^{(0)} \equiv m_0$, and the hopping for which $m_t^{(i)} = 0$ at some $i > 0$ corresponds to the detachment of an atom from the surface. Finally, the probability of remaining at the initial site during the ongoing time step is equal to

$$p_{target}^{(0)} = 1 - p^{m_0} + p^{m_0}\exp(m_0|\varepsilon|/kT)/S, \quad S = \sum_0^{m_c - m_0}\exp\left(\frac{m_t^{(i)}|\varepsilon|}{kT}\right), \tag{1}$$

and the set of probabilities of hopping to the nearest vacant sites is presented by the values

$$p_{target}^{(i)} = p^{m_0}\exp(m_t^{(i)}|\varepsilon|/kT)/S, \quad 0 < i \le m_c - m_0. \tag{2}$$

To recapitulate, the dynamics of the deposited atoms is characterized by two parameters. Random hopping on the surface structure, with surface diffusion coefficient related to p, involves a (free) energy scale Δ , such that

$$p = e^{-\Delta/kT}. \tag{3}$$

Another free-energy scale, , reflects local binding, and we use its magnitude scaled per kT as follows,

$$\alpha = |\varepsilon|/kT. \tag{4}$$

Increasing/decreasing temperature, T, leads to varying the parameters of the model, i.e. α and p, which are correlated to each other by the relation **[62]**

$$p = (p_0)^{\alpha/\alpha_0}. \tag{5}$$

The unit of length in our work is

$$l_0 = a/\sqrt{2}, \tag{6}$$

where a is the lattice constant for the diamond cubic crystal structure. The length l_0 is the distance between neighbor atoms in the [110]-direction.

In our preliminary simulations for carbon-group materials (silicon, Si, and germanium, Ge) with the diamond lattice structure **[54]**, we used reference values $\alpha_0 = 2.7$ and $p_0 = 0.36$ and studied the break-up of nanowires for the following ranges of values

$$\alpha = 2.4 - 3.0 \quad \text{and} \quad p = 0.32 - 0.4. \tag{7}$$

As the conclusion of this section, we would like to discuss the adequateness of the model used to the studied phenomena. As emphasized in earlier studies **[59-69]**, the utilized MC model is mesoscopic and therefore is presently limited in completeness of description of investigated processes. As common for simplified models of particle morphology evolution, our transition rules are not directly related to realistic atom–atom and atom–environment interactions or entropic effects, and, given that we are studying a nonequilibrium regime, we have not made attempts to ensure the detailed balance.

The origin that the results obtained in presented work, as well as in our previous studies, are in good agreement with experimental data is based on the proper choise of the reference parameters α_0 and p_0 for a given crystal structure of synthesized nanoclusters. The criterion for this choice is based on the fact that the dynamics of a nanoparticle with an arbitrary initial shape, calculated on the basis of the rules described above, should lead to a configuration that is close to the Wulff construction corresponding to this crystal structure **[70]**. In general, the insignificant differences in these two configurations are due to the fact that the kinetic processes on the surface of the nanoparticle, which are taken into account in the numerical model, are not taken into account when determining the Wulff construction. Examples of such calculations, after corresponding fitting of the parameters α_0 and p_0, are shown in Supplementary materials, in which the described procedure is followed for FCC and diamond-like crystal structures. The obtained results demonstrate the correctness of determining the equilibrium shape of nanoparticles in comparison with experimental data. Moreover, we found possible physical reasons **[54]** that most natural diamonds have the octahedron shape, which significantly differs from the Wulff construction for such a type of crystal structure (see Suppl. materials). Whether the principle of detailed balance is satisfied in the attained steady states is a problem that requires additional research. (By detailed balance, we mean a certain math requirement related to a generalized property of a system of atoms and not for individual local processes - see subsection 5 in the Suppl. Materials.) The proper fitting of the reference parameters α_0 and p_0 for calculating the equilibrium states allows adequate modeling of the nonequilibrium nanocluster growth.

There are three regimes of particle growth **[59]**. The first of them corresponds to slow growth rates when the concentration of externally diffusing atoms is low. In this case, the time scale of the diffusion of already attached atoms on the cluster surface, τ_D, is much smaller than the time

scale of the formation of new monolayers, τ_{layer}. Then the shape of the growing cluster is close to the Wulff construction. The second regime, $\tau_{layer} \ll \tau_D$, leads to chaotic fast growth and formation of the "strange"/fractal shapes of nanoclusters. Most interesting regime, $\tau_{layer} \sim \tau_D$, corresponds to a "moderately unstable" mode. The growth of clusters is nonequilibrium, but they can be evenly shaped with well-developed faces, as one can see below (see Section 3), but their shapes significantly differ from the Wulff construction. We think that the presented results are creditable because the model used in this moderately unstable mode had demonstrated a very well agreement with the experimental results **[71]**. In the case of BCC lattice (the Wulff construction is rhombic dodecahedron), the shape of synthesized nanoclusters varies in the succession - rhombic dodecahedron⇒truncated cubic⇒cubic that arise in the result of self-consistent dynamics of spatial and surface flows of atoms **[59]**.

Note that more realistic modeling would require prohibitive numerical resources and thus make it impractical to study large enough systems to observe the features of interest in surface structure formation. The model proposed above allows us to simulate the dynamics of systems containing a large number of atoms and establish the main factors that are responsible for the evolution of the morphology of the studied nanosystems.

2.2 Physical approximations of the numerical model. In the presented work we will often compare the obtained result with the results of known experiments **[38,39].** As one can see below, the morphologies of synthesized structures are in good qualitative agreement with the observed reality. Nevertheless, some specific approximations made in the model should be discussed. First of all, the problem of thermal instability of the basic nanowire - which can lead to spontaneous periodic modulations of its surface - complicates the synthesis process. The dynamics of the break-up of nanowires is highly anisotropic [**54]**. In orientation [111] (the nanowire axis is the axis of symmetry of the third-order), the nanowire disintegrates in all temperature regimes: hot ($\alpha = 2.4$ and p =0.4), warm ($\alpha = 2.7$ and $p = 0.36$), and cold ($\alpha = 3.0$ and $p = 0.32$). The break-up of a nanowire in a relatively short time is due to the excitation of surface perturbations with a wavelength of $\sim(4.5 - 5.5)r_0$ because its surface undergoes a roughening transition **[54]**, which is the result of an intense exchange by atoms between the surface and the surrounding vapor of free atoms **[54]**. In this orientation, the factor of roughening transition also largely determines the morphology of the synthesized periodically modulated nanostructures, as described below.

The nanowires with the [100] and [110] orientations (i.e., the symmetry axes of the fourth and second orders, respectively) have the highest thermal stability. They break up only in the hot regime into fragments of $\sim 20r_0$ long. Thus, in the intermediate and cold temperature regimes, the effects of spontaneous periodic modulations of the surface of the basic nanowire do not manifest themselves in the synthesis of nanostructures and we may consider the atoms of the basic nanowire to be stationary. Since accessible computer resources are limited, we simulate the dynamics of the relatively thin basic nanowires (in comparison with those used in [**38,39]** and **[54]**), which may spontaneously modify its surface for a shorter time. Nevertheless, in some

cases, we consider the atoms of these nanowires to be stationary without distorting the main features of the synthesis process.

The second approximation is concerned with the limited size of the computational domain that imposes the short mean free pass, ℓ, of free particles in the computational model compared to the conditions of the experiments of [**38,39]** in which the total pressure (SiH_4+H_2) is varied within the range $0.3-0.6$ Torr (the movement of the SiH_4-molecules is chaotic, temperature $T\sim740-850$ ℃). The mentioned shortening of ℓ is acceptable because the synthesized nanoclusters growth depends on the total flux of free atoms to the nanowire surface, $\Gamma_{surf}^{(+)}$, that can be given by the proper choice of the parameter n_{free}. In turn, the concentration $n_{free}=\beta n_0$, where $n_0=1.4\times10^{-3}$ is the dimensionless unit of free atoms concentration. The parameter β provides the needed level of $\Gamma_{surf}^{(+)}$, so that at the initial stage of synthesis its value exceeds the total flux, $\Gamma_{subl}^{(-)}$, of "evaporating" atoms up to some extent (if $d_0=4$ ($\sim1.6\,nm$ for Ge), then $\Gamma_{surf}^{(+)}\approx\Gamma_{subl}^{(-)}$ at $\beta=1$).

3. Results

Here, we present the results of our numerical experiments, which demonstrate a variety of scenarios for the evolution of the morphology of one-dimensional nanostructures depending on the orientation of the basic nanowire, the supply rate of deposited atoms, and the temperature of the system. These results do not pretend to quantitative agreement of the calculated geometrical parameters of synthesized nanostructures and the characteristic times of their synthesis with experimental data, at least due to limited computing resources (in our work, the largest diameter, d_0, of a nanowire is $4.8\,nm$, while in experiments **[38]** $d\gtrsim30\,nm$). Nevertheless, the regularities that we have established are in complete qualitative agreement with the results presented in [38].

3.1 Dynamics of spatial and surface diffusion fluxes in the synthesis process of ordered one-dimensional structures

Let us consider the physical mechanisms responsible for the disclosed possibility of stabilizing the thermal instability of a nanowire at a sufficient flux density of deposited atoms, $\Gamma_{surf}^{(+)}$, onto its surface. The claim that at a high level of $\Gamma_{surf}^{(+)}$ one should expect the formation of an almost uniform layer of deposited atoms over the thickness is rather clear. More important and problematic is the possibility of formation of individual clusters without significant modifications of the cross-section/diameter of the nanowire between adjacent synthesized clusters. The reality of such a possibility is demonstrated by the data in Fig. 2. Note that, in this case, spontaneous, short-wavelength periodic surface perturbations are associated with the roughening transition effect **[54, 72-73]**, which is caused by the exchange of the nanowire surface with a near-surface layer of "native" sublimated free atoms. These spontaneous modulations of the nanowire surface cause a redistribution of the density of spatial fluxes of

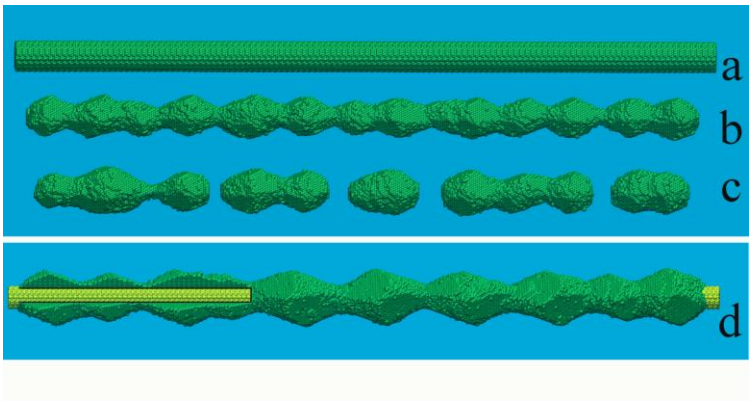

Figure 2. Stabilization of the break-up of a [111] nanowire by a diffusion flux of atoms to its surface. The warm temperature regime ($\alpha = 2.7,\ p = 0.36$, $L = 350$ and $d_0 = 12$ ($4.8\,nm$ for Ge)). Configurations (a), (b), and (c) depict the shape of a nanowire at $t = 0, 3.0,$ and 5.5 ($\times 10^6$) MC steps, respectively; configuration (d) shows the lateral surface of a nanowire with $r = 5$ at $t = 5.5 \times 10^6$ MC steps in the synthesis regime ($\beta = 2.35$). The yellow cylinder represents the initial nanowire shape that contains $N_0 \approx 77 \times 10^3$ atoms; the total number of atoms is $N_t \approx 279 \times 10^3$.

atoms supplied to the system from outside. The intensification of these fluxes into the broadening zones leads to their unstable growth in which the "leaders" of this growth absorb neighboring beads.

In Fig. 2, the break-up of the nanowire is due to surface perturbations with $\lambda \approx 4.5 r_0$ (see configuration (b) depicting 13 beads). At a lower diameter of nanowire (d_0 = 10 rather than 12), the number of beads must be greater than 13 (around 16); however, the external flux of free atoms stabilizes the observed instability (Fig. 2(d)) as a result of the merging of the forming seeds into more extended clusters that corresponds to increasing the effective radius, r_{eff}, of the nanowire

$$r_{eff}/r_0 \approx \sqrt{N_t/N_0} \sim 1.9, \tag{8}$$

where N_0 and N_t are the number of atoms in the nanowire at $t = 0$ and at the end of the synthesis process, respectively. It should be noted that the ratio $\Lambda/r_{eff} \approx 4.5$ (Λ is the distance between the centers of neighboring nanoparticles), which is the result of interaction of the nanowire surface with the spatial fluxes, mimics the ratio $\lambda/r_0 \approx 4.5$ caused by the analogous interaction when the roughening transition arises.

Thus, the synthesized one-dimensional structure can be represented as a result of the dynamics of only deposited atoms on the "frozen" initial nanowire (see the yellow rod in Fig. 2 (d)). A similar conclusion was made by the authors of [38] on the basis of an analysis of numerous experimental

data. The approximation in which the atoms of the basic nanowire may be supposed to be stationary allows us to reveal the features of the dynamics of very extended one-dimensional systems with an acceptable cost of computational resources if the diameter of the basic nanowire is $d_0 \sim 2\ nm$ (the number of deposited atoms, N_t, increases up to 500,000). The result of the corresponding numerical experiment, mimicking the result presented in Fig. 2, is shown in Fig.

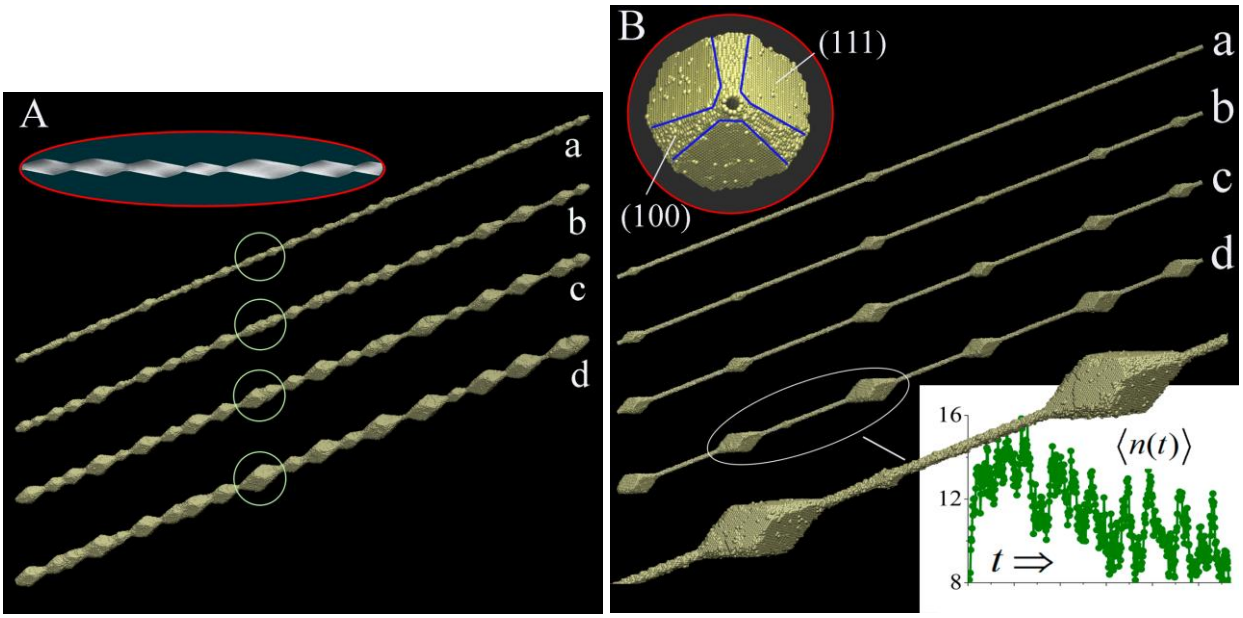

Figure 3. Simulation of the crystal growth of periodic shells on nanowire cores with [111] orientation. (A) Warm regime: $\alpha = 2.7, p = 0.36, = 800, d_0 = 4,$ and $\beta = 2.65$. In subparts (a), (b), (c), and (d): $t = 1.8,\ 3.6,\ 5.4,$ and $7.2\ (\times 10^6)$ MC steps, respectively. The number of atoms at the end of the process is $N_t = 468 \times 10^3$. In green circles, the gradual merger of neighboring shells is shown. The upper inset depicts the experimental Ge-Ge core-shell configuration obtained in [38]. (B) Cold regime: $\alpha = 3, p = 0.32, L = 850,\ d = 4,$ and $\beta = 1.07$. In subparts (a), (b), (c), and (d): $t = 11.45, 17, 30,$ and $56.7\ (\times 10^6)$ MC steps, respectively. The number of atoms at the end of the process is $N_t = 360 \times 10^3$. The upper inset shows the lateral surface of the formed shells. The bottom inset illustrates the dependency of the number of atoms per unit length between two adjacent shells on time during the synthesis process.

3A. (When the diameter of nanowire decreases, the parameter β must be increased to overcome the sublimation flux from its surface). Surface perturbations at the initial stage of synthesis (see configuration (a) in Fig. 3A) may be identified with the instability of epitaxial growth **[74]**. The later stage of synthesis (configuration (d)) is characterized by inevitable merging (absorption of each other) of the previously formed nanoclusters into larger ones.

In the cold synthesis mode (thermal instability is largely suppressed), more complicated scenarios of long-range self-organization of the forming nanoclusters can be realized (see Fig. 3B and Fig. 4A; the distances between nanodrops significantly exceed their sizes).

In this case, at low flux densities $\Gamma_{surf}^{(+)}$ ($\beta \leq 1.1$), the basic nanowire is covered with a "surface gas" of deposited atoms, which is in a metastable state and in which the nuclei of a new phase - primary nanoclusters - are formed (see Fig. 4B, configuration (c)). The subsequent growth of each of these nuclei is accompanied by competition between them during the absorption of individual surface atoms in the intermediate regions. As a result of such competition, single

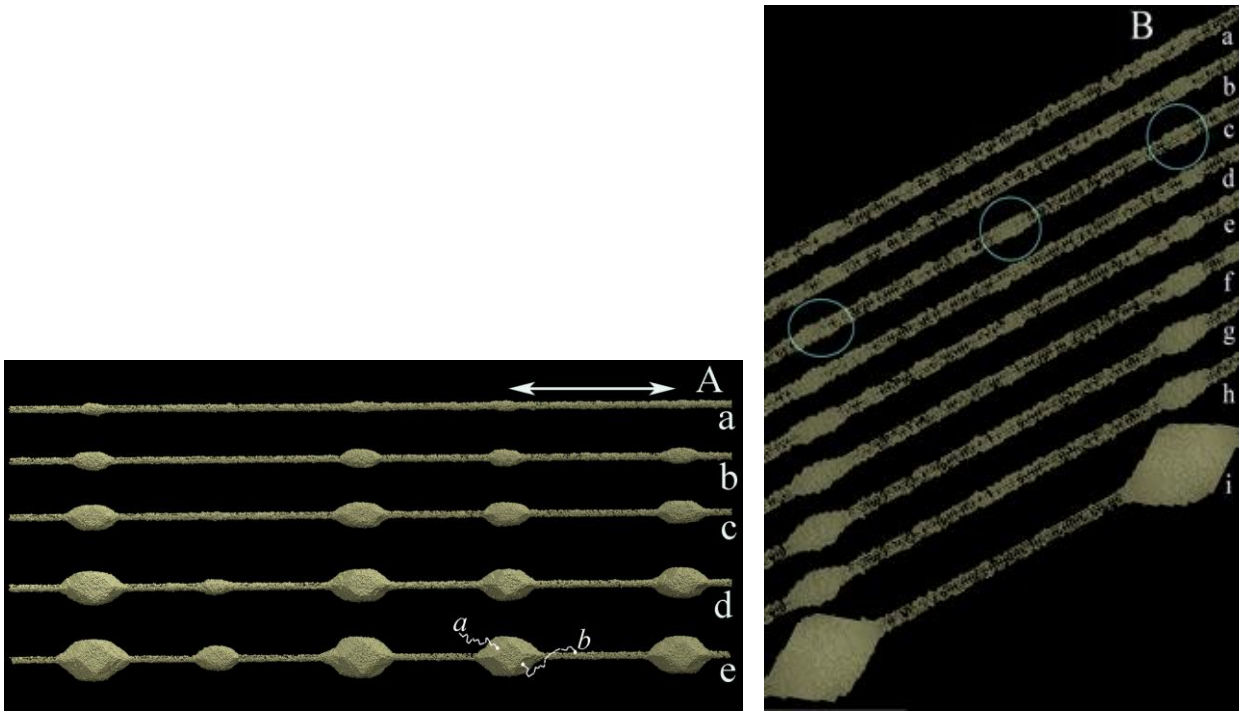

Figure 4. Growth of periodic shells on nanowires with the [100]-orientation. Cold regime: $\alpha = 3.0, p = 0.32,\ L = 600, d = 4,$ and $\beta = 1.1$. (A) Subparts (a) to (e) depict the configurations of the system at $t = 8, 12, 16, 20, 24.9$ ($\times 10^6$) MC steps, respectively. The number of adsorbed atoms at the end of the process is $N_t \approx 322 \times 10^3$. (B) Dynamics of adsorbed atoms in the gap between two adjacent nanoclusters on the right (this interval is marked by a white arrow in part A). The atoms that originally constitute the nanowire are not shown. Subparts (a) to (i) are the snapshots of the region taken at $t = 4, 5, 6, 7, 8, 9, 10, 11,$ and 20 ($\times 10^6$) MC steps, respectively. The seeds of the potential shells are shown inside cyan circles. The middle seed (see configuration (c)) does not survive in competition with its neighbors.

nuclei of the new phase turn out in zones of low surface density of the surrounding deposited atoms and gradually disappear, i.e. the adjacent nuclei absorb each other due to the well-known Ostwald ripening effect (see configurations (c) to (h) in Fig. 4B, and Video file "Nuclei_Competition" in the Supplementary Materials).

Note that a decrease in the average linear density, $\langle n_s(x,t)\rangle_x$, of deposited atoms in the regions between the nuclei occurs when their sizes are small in height (see Fig. 3B, the lower inset; the maximum value of $\langle n_s(x,t)\rangle_x$ is attained in configuration (a)), so that the 'shadow effect' discussed below does not manifest itself. Thus, the decrease in $\langle n_s(x,t)\rangle_x$ is due to the

increasing fluxes of surface diffusion to growing nuclei, since the probability of irreversible capture of single surface atoms increases as a result of gradually increasing the number of their bonds with growing nanoclusters. Consequently, the formation of a high degree of regularity in the chain of clusters formed in the initial stage is based on their 'long-range interactions' through surface diffusion flows.

When the heights of growing clusters are comparable with the radius of the basic nanowire, the effect of redistribution of spatial diffusion fluxes of free atoms arises, which leads to the inhomogeneity of the $\Gamma_{surf}^{(+)}$ value along the nanowire. The physical interpretation of this effect is straightforward. Suppose that at a low cluster height, some free atom reach the nanowire surface, moving along the trajectory a-b (see configuration (e) in Fig. 4A). The growth of a cluster in time may lead to the closure of such trajectories on its surface. In fact, growing nanoclusters screen parts of the spatial diffusion fluxes to the surface of the nanowire sections between them. This well-known shadow effect can effectively not only prevent the formation of new nuclei, but also destroy the already-formed ones (see Video-files "Nuclei_Competition", "Origination-Dilution" and Fig. S2 in the Supplementary Materials). In a model problem (two balls with a radius of 10 units are located on a nanowire with a radius of 2 units and are at a distance of 200 units from each other), the density of spatial diffusion fluxes to the surface of the wire in the central region between the balls decreases by ~ 10% in comparison with the result obtained in the absence of balls. It is this shadow effect that causes a significant decrease in $\langle n_s(x,t)\rangle_x$ at later stages of synthesis (see the lower inset of Fig. 3B). If, after the formation of large clusters, we increase the supply of free atoms to the system (i.e. increase β), then the gap between the primary clusters can be filled with small-scale beads (this result was demonstrated in the experimental work [**39**] and in our numerical experiments - see Fig. S1 in the Supplementary Materials).

For qualitative estimations in the future, we note that the idea of the inhomogeneity of the distribution of the value $\Gamma_{surf}^{(+)}$ over the surface of the nanocluster can be given by a solution to the electrostatic problem of finding the electric field strength, E_{surf}, on its surface, which is considered to be charged and conducting, inasmuch as $\Gamma_{surf}^{(+)} \sim E_{surf}$. As a rule, the highest flux density $\Gamma_{surf}^{(+)}$ (the value E_{surf}) is achieved in the regions of high surface curvature (sharp vertices and sharp edges of nanocluster).

The distance between clusters, l_{int}, can be easily estimated in the approximation of constant sublimation flux density from the nanowire surface, $\Gamma_{subl}^{(-)}(x)$, along it. The equations

$$D_s \frac{d^2 n_s}{dx^2} + \Gamma_{surf}^{(+)} - \Gamma_{subl}^{(-)} = 0;\ n_s(x=0) = n_s(x=l_{int}) \approx 0 \qquad (9)$$

describe the distribution of $n_s(x)$ along the nanowire in a quasi-stationary state. The boundary conditions correspond to the assumption that nanoclusters irreversibly absorb the drifting surface atoms, D_s is the diffusion coefficient of these atoms. Therefore,

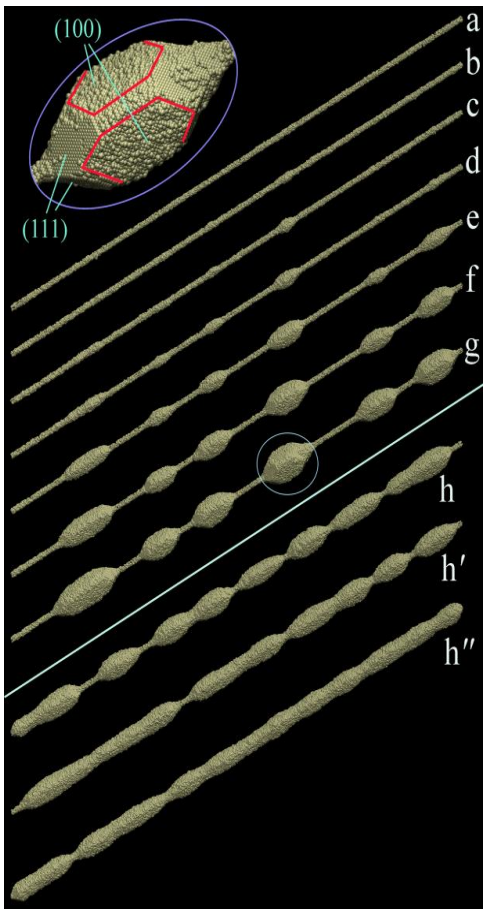

Figure 5. Simulation of synthesis of periodic shells on nanowires with the [100]-orientation. Warm regime: $\alpha = 2.7, p = 0.36,\ L = 600$, and $d_0 = 4$. Subparts (a) to (g) show the dynamics of the system at $\beta = 2.5$; $t = 1, 2, 3, 4, 6, 8, 10$ ($\times 10^6$) MC steps; $N_t \approx 322 \times 10^3$. The inset at the top shows the shape of one of the nanoclusters marked with a circle in configuration (g). Configurations (h), (h′), and (h′′) represent the states of the system (for greater values of β) at times when the number of deposited atoms reaches $N_t = 300 \times 10^3$; Accordingly, $\beta = 2.55, t = 6.65 \times 10^6$ (h); $\beta = 2.6, t = 5.55 \times 10^6$ (h′); $\beta = 2.7, t = 4.40 \times 10^6$ (h′′).

$$n_s(x) \approx \frac{\Gamma_{surf}^{(+)} - \Gamma_{subl}^{(-)}}{2D_s} x(1 - x/l_{int}),\ n_s^{(max)}\left(x = \frac{l_{int}}{2}\right) = \frac{\Gamma_{surf}^{(+)} - \Gamma_{subl}^{(-)}}{8D_s} l_{int}. \quad (10)$$

New nuclei (nuclei of second generation; see configurations (b), (c), and (d) in Fig. 4A) can reach a critical size if the maximum density of deposited atoms between neighboring clusters, $n_s^{(max)}$, exceeds some critical value $n_s^{(cr)}$: $n_s^{(max)} > n_s^{(cr)}$. That is, the characteristic distance between clusters can be estimated as

$$l_{int} \sim D_s / \left(\Gamma_{surf}^{(+)} - \Gamma_{subl}^{(-)}\right). \quad (11)$$

Approximate dependence (11), $l_{int}(\Gamma_{surf}^{(+)})$, where $\Gamma_{surf}^{(+)} \sim \beta$, rather accurately reflects the sensitivity of the distances between clusters to insignificant changes in parameter β. The results presented in Fig. 1 (configuration (a)) and Fig. 4 (configuration (e)) were obtained under the same synthesis conditions ($\alpha = 3.0, p = 0.32$, $d = 4$, and $\beta = 1.1$). When comparing these data, it can be seen that the average values of the distances between clusters, $\langle l_{int} \rangle$, are quantities of the same order (some variations in $\langle l_{int} \rangle$ are inevitable due to the randomness of the processes occurring). However, small changes in parameter β from 1.1 to 1.07 lead to an increase in $\langle l_{int} \rangle$ by more than 2.5 times (see configuration (b) in Fig. 1), which corresponds to estimate (11) that is very sensitive to the difference $\Gamma_{surf}^{(+)} - \Gamma_{subl}^{(-)}$ for its low values.

The desired periodicity of synthesized clusters can be formed at different temperatures by varying the value of $\Gamma_{surf}^{(+)} \sim \beta$. The average value $\langle l_{int} \rangle$ for configuration (g) in Fig. 5 and configuration (a) in Fig. (1) is practically the same, although the synthesis was carried out in different temperature conditions. In the warm mode, the sublimation flux density $\Gamma_{subl}^{(-)}$ increases, therefore, according to estimate (11), parameter β should be increased ($\beta \geq 2.5$ in Fig. 5). An increase in the flux density $\Gamma_{surf}^{(+)}$ (see configurations (h), (h′), and (h″) in Fig. 5) leads to the narrowing of the gaps between adjacent clusters up to the formation of an almost uniform basic wire coating. This effect is observed in experiments [38] and does not require detailed explanations of its physical mechanisms.

3.2 Dependence of the shape of synthesized nanoclusters on the orientation of the nanowire.

At the later stages of synthesis, when the sizes of the formed clusters change rather slowly, the evolving one-dimensional system can be considered to be in equilibrium with a near-surface layer of free atoms, so that at each moment of time its free energy is minimal for a given morphology. The equilibrium state of an isolated nanoparticle corresponds to the minimum of its surface energy, which is achieved when the nanoparticle shape is approximated by the Wulff construction **[70]**. This shape is bounded by the planes with the lowest surface energy densities, $\sigma_{[mnl]}$. The distance of each face, $\delta_{[mnl]}$, from the common center is proportional to the corresponding value $\sigma_{[mnl]}$, i.e. $\delta_{[mnl]} / \sigma_{[mnl]} = const$.

In the case of Si, the Wulff construction is built mainly by faces [111], [100], and [110] ($\sigma_{[111]} < \sigma_{[100]} < \sigma_{[110]}$) - see Fig. 6 where a rough representation of it is given in the form of a truncated octahedron. It should be noted that such a nanodroplet shape approximation does not take into account kinetic processes on the particle surface and in the near-surface layer. If exchange with the surrounding vapor of free atoms is blocked (only surface diffusion forms the equilibrium shape of a particle), then this shape is close to octahedron [54] (this is the shape that is characteristic of most natural diamonds).

If a nanocluster grows on a nanowire, then the flows of deposited atoms onto its surface differ from flows that form an isolated particle. First, surface diffusion of deposited atoms along the basic nanowire obviously determines the anisotropy of the flows that provide cluster growth. Second, the corresponding deformation of the cluster (relative to the Wulff construction) causes a redistribution of spatial diffusion fluxes. Both of these factors lead to significant shape modifications of synthesized nanoclusters (see Fig. 1B).

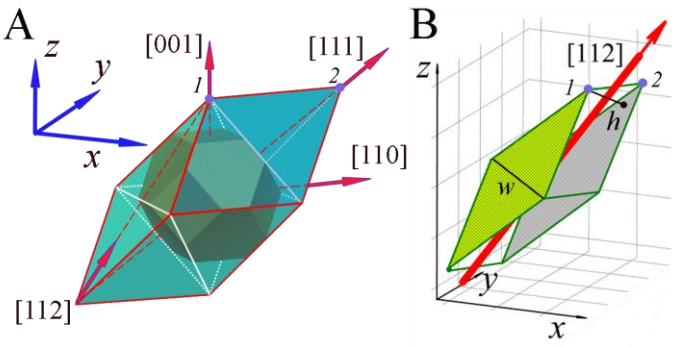

Figure 6. Schemes for the explanation of shapes of synthesized nanoclusters. (A) The truncated octahedron, inscribed in a rhombohedron, presents the Wulff construction for the diamond cubic crystal lattice. The rhombohedron itself is an approximation of nanoclusters shape when the basic nanowire is oriented in the [111]-direction. (B) The shape of formed clusters in the case of [112]-orientation.

The shape of clusters for the [111]-nanowire orientation is easily predictable. Fluxes of deposited atoms from the adjacent nanowire fragments elongate the nanoclusters in this direction, which, in its turn, enhances the flow of free atoms to the vertices of the formed rhombohedron, limited mainly by six faces of the [111]-type (see Figs. 1B(c) and 3B). A similar situation is realized in the [100]-nanowire orientation (see Figs. 4 and 5). The synthesized nanoclusters mimic the Wulff construction elongated along the [100]-type axis.

If a wire with the [111]-orientation is gradually turned in the plane (-110) to the [112]-orientation, the transformation of the shape of growing nanoclusters corresponds to a continuous reduction of the edges of rhombohedron type (1-2) (see Fig. 6A) to some limiting size (see Fig. 6B). The results of the corresponding numerical experiments are presented in Fig. 7. Note that the ratio of the growth rate of height, h, of flattened nanoclusters to the rate of change in the characteristic size, w, of rhomboid lateral [111]-faces (see Fig. 6B) varies with time and depends on parameters β (the flux density of free atoms on these faces), p (the value $p(T)$ determines the surface diffusion coefficient D_s), and finally on the value w itself. If the average deposition time of a free atom, τ, to the wide (111)-facet is greater than the diffusion time of the deposited atom along this facet, τ_D, i.e. $\tau > \tau_D$, then $\frac{dw}{dt} > \frac{dh}{dt}$ because the deposited atoms intensively move to the edges of the wide faces without enough time to form new layers on them. The condition,

$\tau > \tau_D$, for the dominance of the broadening, w, of the nanocluster over its thickening, h, has the form

$$w < w_{cr} \sim \sqrt[4]{D_s/\beta}, \tag{12}$$

if we take into account the estimations $\tau \sim 1/(\beta w^2)$ and $\tau_D \sim w^2/D_s$. Thus, the cluster switches to regime of predominant growth in its height when $w > w_{cr}$. This rather qualitative statement is demonstrated when comparing the ratio h/w for the options presented in Fig. 7A ($p = 0.32, \beta = 1.1$) and Fig. 7B ($p = 0.36, \beta = 2.6$).

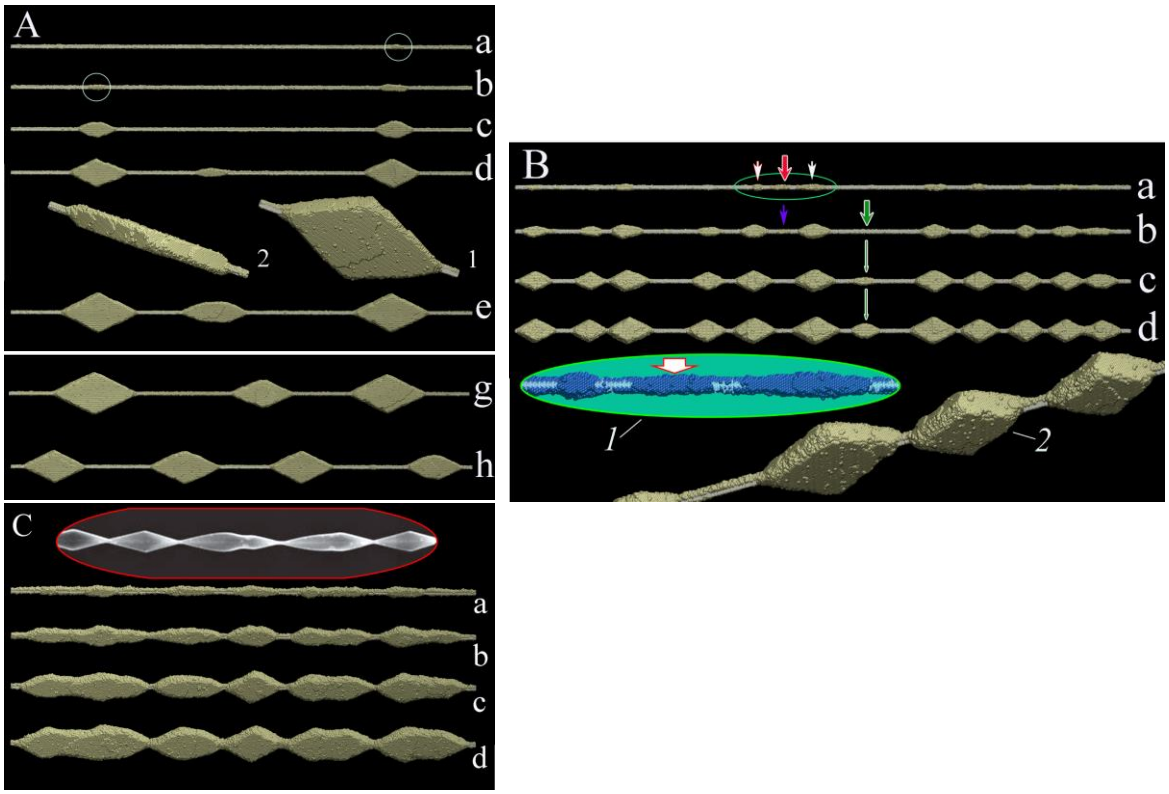

Figure 7. Nanocluster growth in a diffusion mode on a [112]-nanowire. (A) Synthesis in cold regime: $\alpha = 3,\ p = 0.32,\ L = 780, d_0 = 4$ and $\beta = 1.1$. In sub-parts (a) to (e): $t = 2, 3.5, 5, 6.5$ and $8\ (\times 10^7)$ MC steps, respectively ($N_t \approx 367 \times 10^3$). Insets 1 and 2 show side and top views of one of the clusters illustrated in configuration (d). Sub-parts (g) and (h) present the results of numerical experiments with different random number sequences. In both the final states $N_t = 367 \times 10^3$; $t = 8.01 \times 10^7$ and 6.3×10^7 MC steps. (B) Warm regime: $\alpha = 2.7, p = 0.36,$ $L = 1000, d_0 = 4,$ and $\beta = 2.6$. In sub-parts (a) to (d): $t = 0.3, 0.6, 0.9,$ and $1.17\ (\times 10^7)$ MC steps, respectively ($N_t = 620 \times 10^3$). Red arrow marks the nucleus that was absorbed by its neighbors, whereas olive arrows show the region where a nanocluster of the second generation is formed. Inset 1 illustrates the enlarged image of the nanowire piece marked by an ellipse in configuration (a). Inset 2 shows the shape of three adjacent nanoclusters at the end of the process. (C) Warm regime: $\alpha = 2.7, p = 0.36,\ L = 780, d_0 = 4,$ and $\beta = 2.75$. In sub-parts (a) to (d): $t = 0.2, 0.4,\ 0.6,$ and $0.775\ (\times 10^7)$ MC steps, respectively ($N_t \approx 396 \times 10^3$). The upper inset presents one of the experimental results [38] (the images of Si nanoclusters, deposited on a Si nanowire).

In the first case, for a larger average number of atoms, $\langle n_{cl} \rangle$, in one cluster ($\langle n_{cl} \rangle_{(7A)} \approx 1.1 \times 10^5$ vs. $\langle n_{cl} \rangle_{(7B)} \approx 0.51 \times 10^5$) the value of h/w is less due to the manifestation of two self-consistent factors. With the slower supply of free atoms to the system, $\beta = 1.1$, the threshold $w_{cr}(\beta = 1.1) > w_{cr}(\beta = 2.6)$, which determines the predominance of growth of the cluster in width to higher values of w. In turn, when the ratio h/w decreases, then the density of the diffusion flux, $\Gamma_{surf}^{(+)}$, at the periphery of the diamond-shaped cluster increases with respect to its value at the center of the wide (111)-face. This non-obvious statement can be easily established based on the analogy noted above between the distribution of $\Gamma_{surf}^{(+)}$ and the electric field E_{surf} over the cluster surface, which is considered to be charged and conducting. It is known that as the flat configuration becomes thinner (smaller values of the parameter h/w), E_{surf} increases at its edges.

In the [112]-nanowire orientation, the scenarios of self-ordering of the synthesized nanoclusters are the same as in the above cases of [111]- and [100]-orientations. Figures 7A and 7B show both the formation of delayed clusters of the second generation and the absorption by the nearest neighbors of the cluster that has arisen between them (see inset 1 and configurations (b), (c), and (d) in Fig. 7B; video file "Nucleus_Dynamics" in the Supplementary Materials shows the full dynamics of one of the short-lived clusters from the moment of origination to subsequent dissolution). An increase in the flux of free atoms to the nanowire surface (see Fig. 7C) reduces the gaps between clusters and leads to a scatter in their size and shape, while in the slow growth modes (see Figs. 3B, 4A, and 7A) a higher level of order is noticeable in a synthesized system.

The shape of the synthesized nanoclusters in the [110]-orientation of the nanowire mimics the shape of short fragments of a long nanowire, the surface of which corresponds to the minimum surface energy. Such a surface will be formed by the Wulff construction (see Fig. 6) if it is being moved along the [110]-axis: the upper/lower faces are represented by (100)-type planes, and the side surfaces are formed by two pairs of adjacent (111)-type planes. The distance of each of the six faces $\delta_{[mnl]}$ from the wire axis is proportional to the corresponding value of the surface energy density $\sigma_{[mnl]}$. According to the experimental values of $\sigma_{[mnl]}$ for Si **[70]**, the ratio $\sigma_{[100]}/\sigma_{[111]} \approx 1.1$. In our numerical experiments, the distance ratio $\delta_{[100]}/\delta_{[111]}$ is of the order of 1.45 (see the rightmost inset in Fig. 8A). The observed deviation is associated, as we have already noted above, with kinetic processes both on the surface of the nanocluster and in the near-surface of free atoms. Deposited on the (111)-facets atoms roll to (100)-facets because of its high coefficient surface diffusion, $D_{s,(111)}$. The cluster growth along the [100]-direction redistributes diffusion fluxes near its surface so that they increase near its upper / lower sharp "edge", which finally leads to the above inequality $\delta_{[100]}/\delta_{[111]} > \sigma_{[100]}/\sigma_{[111]}$.

The length of the formed [110]-clusters, l_{clust}, significantly exceeds their characteristic transverse size, w, so that the l_{clust}/w ratio is noticeably higher than the analogous parameter for other orientations. The observed difference is associated with different diffusion coefficients and

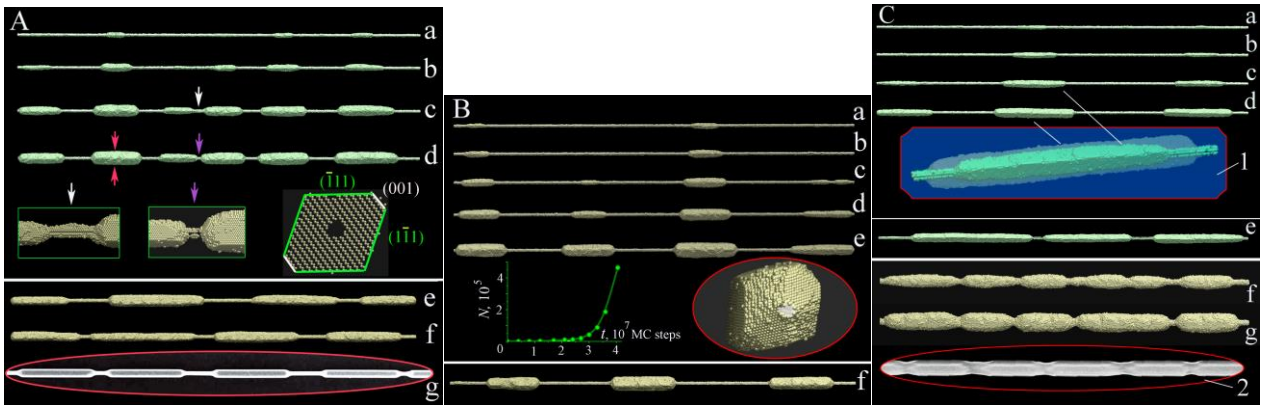

Figure 8. Growth of nanoclusters on nanowires with the [110] orientation. (A) Synthesis in the warm regime: $\alpha = 2.7, p = 0.36,\ L = 900,\ d_0 = 4,$ and $\beta = 2.7$. In sub-parts (a) to (d): $t = 0.5,\ 0.75,\ 1.1,$ and $1.275\ (\times 10^7)$ MC steps, respectively ($N_t = 490 \times 10^3$). In the insets: changes in time of the interval between two clusters marked in configurations (c) and (d) with white and purple arrows. Inset in the right shows the cross-section of the nanocluster indicated by red arrows. Sub-parts (e) and (f) depict two random system configurations with $d_0 = 5$ and $\beta = 2.375$ at $t = 3.13$ and $2.98\ (\times 10^7)$ MC steps, where $N_t = 441.6 \times 10^3$ and 443×10^3, respectively. Sub-part (g) represents the experimental result for Si [38]. (B) Warm regime: $\alpha = 2.7, p = 0.36,\ L = 900,\ d_0 = 4,$ and $\beta = 2.6$. In sub-parts (a) to (e): $t = 27, 30, 33, 36,$ and $40.5\ (\times 10^7)$ MC steps, respectively ($N_t = 464 \times 10^3$). Sub-part (f) shows the result of another numerical experiment with different random number sequence: $t = 29.4 \times 10^6$ MC steps and $N_t = 416.5 \times 10^3$. (C) Results presented in sub-parts (a) to (e) are associated with the cold regime, where $\alpha = 3, p = 0.32,\ L = 900,\ d_0 = 4,$ and $\beta = 1.2$. In sub-parts (a) to (d): $t = 14, 21, 28, 35.72\ (\times 10^6)$, and $N_t = 201.3 \times 10^3$. In sub-part (e), the result of another MC simulation is presented, where $t = 40 \times 10^6$ MC steps and $N_t = 321.4 \times 10^3$. Configurations (f) and (g) represent the hot regime where $\alpha = 2.4, p = 0.4,\ L = 480, d_0 = 5,\ \beta = 5.7;$ and $t = 3.0$ and $4.5\ (\times 10^6)$ MC steps, respectively ($N_t = 319 \times 10^3$). Inset 1 demonstrates the growth of the central nanocluster with time. Inset 2 presents one of the experimental results [38].

different binding energies of deposited atoms at the lateral surface of nanoclusters and at its end-walls. This difference is most easily demonstrated by comparing the nanocluster shapes synthesized on the nanowires with the [110]- and [100]-orientations.

In the first case, the lateral surface of the nanoclusters (formed by the facets that are parallel to the nanowire axis) is predominantly formed by the (111)-type faces while in the second one (i.e. the [100]-orientation) the nanoclusters are bounded by the [100]- and [110]-types planes (see inset in Fig. 5; we have already presented their shape above as the Wulff construction extended along the [100]- axis). The binding energy of the individual atoms deposited at densely packed [100]- and [110]-facets is higher than in the case of deposition to the [111]-facet. Thus, being rather densely packed the lateral surface of nanoclusters growing on the [100]-nanowire is characterized by both lower probability of sublimation and slower drift of single deposited atoms along that surface to the nanocluster end-walls. At the same time, four (111)-facets that form these end-walls (see inset in Fig. 5) support the intensive drift of the atoms, deposited onto them, to the lateral nanocluster surface. Finally, the abovementioned factors result in the bead-like shape of [100]-nanoclusters. In the case of [110]-orientation, the opposite effects (intensive drift off lateral surface to end-walls, higher intensity of sublimation and lower back drift from end-

walls, which include the fragments of (100)-facets) result in dominating growth of nanoclusters along the nanowire (see inset 1 in Fig. 8C). Moreover, the initial elongation of [110]-clusters is stimulated by the redistribution of space diffusive fluxes to its ends, which mimics increasing the corresponding field strength, E_{surf}, when the ratio w/l_{clust} for a charged conducting "nail" decreases.

The correspondence of the results of our modeling to the experimental data (see Figs. 1, 3, and 7) is again shown in Figs. 8A and C. Note that, configurations (f) and (g) in Fig. 8C are obtained in the "hot" temperature regime when [110]-nanowire becomes sensitive to the thermal instability, and the mobility of the basic nanowire atoms is taken into account. Nevertheless, a dense diffusive flux of free atoms has suppressed this instability. It is interesting that the elements of the formed sausage-like structures are connected by short deep bottlenecks, which are conserved for a long time as it realizes in the case of [111]-nanowire orientation (see Fig. 2).

3.3 Effects of non-uniform in time rate of supply of free atoms

The analysis of the above results shows that the ordering of the synthesized clusters is due to two mechanisms. The first is related to the surface diffusion of deposited atoms. Nuclei, the size of which exceeds the critical value, create "diffusive" zones (zones of intense absorption of single atoms) with a characteristic size, $\mathcal{L}_{diff}$, that determines the minimum distance between adjacent synthesized nanoclusters or, in other words, the primary self-ordering parameter. Thorough analysis of the data presented in Figs. 3B, 4A, 7A, 7B, and 8B suggests that at the initial stage of synthesis, the most probable distance between neighboring nuclei is around $\sim 2\mathcal{L}_{diff}$ that minimizes the overlap of individual diffusive zones and ensures a steady growth of the "surviving" nuclei. Nevertheless, the formation of second-generation clusters among primary clusters at later stages of synthesis is possible.

The second ordering mechanism - the redistribution of spatial diffusion fluxes (creating a "shadow" in the intercluster gaps) - is effectively switched on only at sufficiently large transverse (relative to the nanowire) cluster sizes. Such shielding (the shadow effect) at the later stages of synthesis can lead to the dissolution of small clusters formed in the gaps that present a specific time-delayed self-ordering mechanism. Nevertheless, the primary self-ordering is determined by the surface diffusion processes. That is, the aforementioned mechanisms of self-organization are most efficiently manifested at different stages of synthesis, which does not always ensure an explicitly expressed ordering in the chain of nanoclusters.

Here, we propose synthesis modes in which both self-ordering mechanisms are activated without time shifts relative to each other that lead to a noticeable increase of regularity in the arrangement of nanoclusters. This method can be especially effective when originating maximum number of single nanoclusters for a given nanowire length as it is shown in Figs. 9D and E. The problem of generating a chain of densely packed clusters (as shown in Fig. 3A(d) and Fig. 5(h)) is related to the fact that such a configuration of the system can be synthesized only at

high densities $\Gamma_{surf}^{(+)}$. However, in this case, the probability of a chaotic distribution of the nuclei along the wire during epitaxy is high **[75]**. Suppression of this chaos due to the spontaneous excitation of short-scale perturbations, associated with the development of thermal instability of the basic nanowire (see Fig. 2), is also problematic since the synthesis time is usually shorter than the characteristic time of this instability **[38]**. The proposed strategy for solving the discussed problem is as follows. At the initial short-term stage of synthesis, create a dense set of nuclei on the nanowire, the locations and sizes of which can be rather random, by utilizing the intense flux density, $\Gamma_{surf}^{(+)}$. Then gradually reduce the supply of free atoms into the system. Such a trick intensifies the competition for survival in the created nuclei system that will be carried out not only by surface diffusion fluxes, but also by the shadow effects from these relatively low, yet densely located, nuclei. Finally, the value $\Gamma_{surf}^{(+)}(\beta)$ is to be increased up to some middle level after establishing self-ordering and then keep on the nanoclusters synthesis to the required size.

The effectiveness of the controlled variation $\Gamma_{surf}^{(+)}(t) \sim \beta(t)$ in time is shown in Fig. 9. The nanowire is oriented along the vector, which coincides with the bisector of directions [112] and [1-10] (the "bisector"-orientation), i.e. lies in the plane (-1-11) similar to the [112]-nanowire (see the Supplementary Materials, Fig. S4). With the unchanged in time parameter $\beta(t) = 2.6$, the result for the [112]-nanowire (see Fig. 7B) is relatively irregular in distribution of the random value Λ (Λ is the distance between centers of neighboring nanoclusters). At the same time, a step-wise variation $\beta(t)$ (see Fig. 9A, time regime (*1*)) leads to a more regular self-ordering (see Fig. 9B). In each of the five realizations, the dynamics of the system moves along a random "trajectory" with a different number of finally synthesized nanoclusters that, however, are settled with regularity in distances between them. Fig. 9C shows the dynamics of the number of atoms in the atomic layers (oriented perpendicularly to the nanowire axis) along the nanowire during the most important stage to originate a stable self-ordered nuclei chain for their growth in sequel.

The generation of a larger number of clusters for the same nanowire length can be realized at large $\beta(t)$ values at the initial stage of synthesis. However, the dynamics of the system of numerous primary nuclei must be controlled in such a way that larger ones are not subsequently in a clear advantage in the competition for survival compared to smaller nuclei. If this is not ensured, the final configuration of the system will be largely determined only by these privileged nuclei rather chaotically located on the nanowire. The results of our numerical experiments show that the exponential reduction of parameter β as a function of time,

$$\beta(t) = \beta_{st} + \Delta\beta \times \exp(-t/\tau), \tag{13}$$

is more practical for the synthesis to be rather controlled (see Figs. 9D, E and the Video-file "Synthesis_in_Exp. regime" in the Supplementary Materials). The nanowire configurations presented in Figs. 9D and E are obtained by utilizing the exponential $\beta(t)$-protocols (*2*) and (*3*) (see Fig. 9A), respectively. The set of nuclei formed at the initial stage of synthesis (see the distribution $n(l)$ in Fig. 9E(a)) "clears" over time from irregularities of various sizes (rectangles

mark the primary nuclei that disappear in competition with nearest neighbors, which "attract" the space diffusive fluxes to their peaks). The surviving nanoclusters set explicitly correlates with the subsequent nanowire shape (see Fig. 9E). A higher value of $\beta(t)$ at the initial stage of synthesis (compare the time-protocols (*2*) and (*3*) for $\beta(t)$ in Fig. 9A) leads to a larger average number of formed nanoclusters (see Fig. 9D and configuration (d) in Fig. 9E). It should be noted that the choice of the parameters $\Delta\beta$ and τ for a given average value $\langle\beta\rangle$,

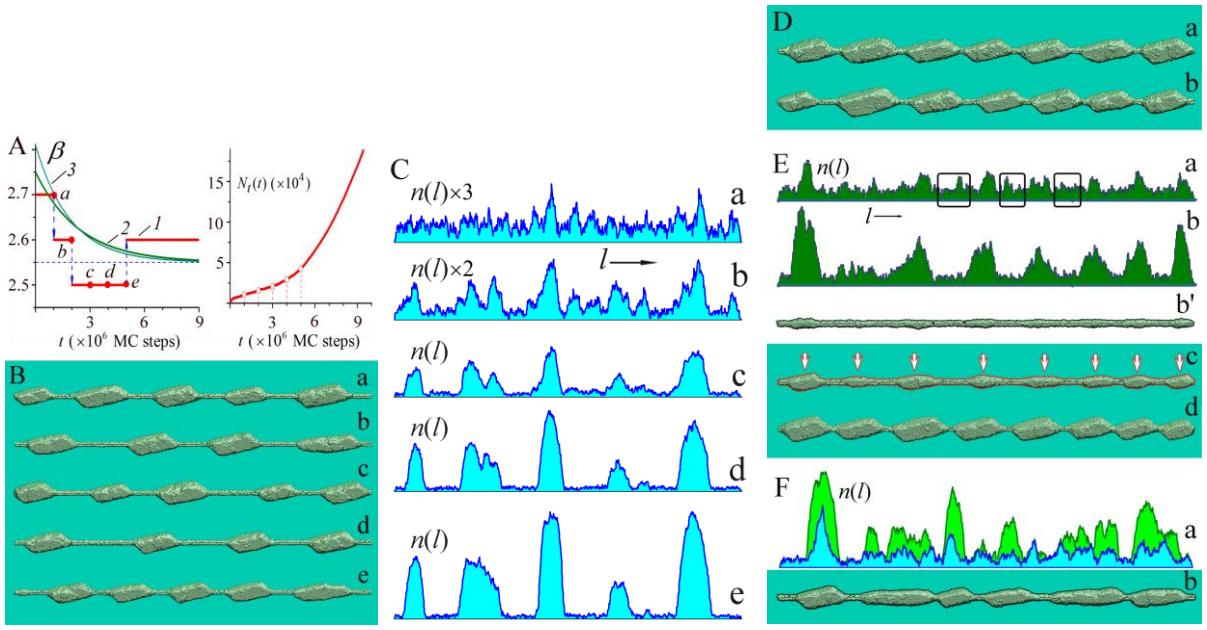

Figure 9. Synthesis of periodic nanoclusters on nanowires with "bisector"-orientation. Warm regime: $\alpha = 2.7, p = 0.36,\ \ L = 500,$ and $d = 4$. (**A**) Three different time-dependencies of the parameter β used in our numerical experiments, and a characteristic growth of the number of deposited atoms, $N_t(t)$, in time for the stepwise regime, i.e. regime (*1*); white circles correspond to time moments (a) to (e) marked in the dependency (*1*). In the exponential regimes (*2*) and (*3*) $\beta = 2.55 + 0.2 \times \exp(-t \times 10^{-6}/2.4)$ and $\beta = 2.55 + 0.26 \times \exp(-t \times 10^{-6}/1.9)$. (**B**) Final configurations obtained by using five different random number sequences for the stepwise regime (*1*). For configurations (a), (b), (c), (d), and (e) the times of synthesis are $t = 9.4,\ 9,\ 11,\ 9.3,$ and $9\ (\times 10^6)$ MC steps and the final numbers of deposited atoms are $N_t = 190, 169, 185, 148,$ and $153\ (\times 10^3)$ respectively. (**C**) Dynamics of the dimensionless number of atoms in atomic layers along the nanowire, $n(l)$, for final configuration (a) shown in part (B). Distributions (a), (b), (c), (d), and (e) correspond to the time moments marked by a, b, c, d, e in part (A). (**D**) Two random configurations of the nanowire for the exponential regime (*2*): for configurations (a) and (b) $t = 8.7 \times 10^6$, $N_t = 254 \times 10^3$ and $t = 9.3 \times 10^6$, $N_t = 225 \times 10^3$, respectively. (**E**) Characteristic dynamics of the nanowire surface for the exponential regime (*3*). Diagrams (a) and (b) present the distributions of $n(l)$ at time moments $t = 0.5 \times 10^6$ and $t = 10^6$ MC steps, respectively (rectangles mark the accumulations of deposited atoms the growth of which is suppressed in time); configurations (b′), (c), and (d) present the nanowire shapes at time moments $t = 1, 2, 9\ (\times 10^6)$ MC steps, respectively (the corresponding numbers of deposited atoms N_t are equal to 17, 55 and 235 $(\times 10^3)$). (**F**) Results for a sharper in time exponential regime: $\beta = 2.55 + 0.26 \times \exp(-t \times 10^{-6}/1.7)$. (a) Distributions $n(l)$ at time moments $t = 1.2 \times 10^6$ and 2.5×10^6 MC steps, restectively. (b) The nanowire shape at $t = 6 \times 10^6$ ($N_t = 127 \times 10^3$).

$$\langle \beta \rangle = \tau_{synt}^{-1} \int_0^{\tau_{synt}} \beta(t) dt, \qquad (14)$$

(τ_{synt} is the synthesis time) should be optimized for obtaining the best result. For example, with an excessively short time parameter τ in Eq. (13), the regularity in the synthesized structure of nanoclusters is noticeably reduced (see Fig. 9F). The physical reasons for the observed effect are discussed at the beginning of this section.

4 Conclusions

The self-organization mechanisms we have considered in the synthesis of one-dimensional ordered structures are based on a wider class of physical processes than in the case of generation of highly- structured layers or sculptured films by the well-known method of oblique angle deposition (OAD) **[76, 77]**. In this method, the main factor controlling the dynamics of the morphology of growing singular nanostructures (zigzag, helical, and s-shaped nanocolumns) is the shadow effect in its simplest manifestation. Deposited atoms fall onto the substrate, which is covered by initially formed nuclei, in the ballistic mode at a certain angle. Under such conditions, the zones behind the ordered protuberances on the substrate are inaccessible for rectilinearly moving atoms, since they are in the geometric shadow. Moreover, the OAD of thin films on patterned substrates is carried out at low temperatures, when the manifestation of any diffusion processes is excluded.

In the case considered in this paper, it is surface diffusion that leads to the formation of primary nuclei that are rather chaotically located on the nanowire. Each of these nuclei creates "surface shadow regions" - diffusive zones - the overlap of which leads to competition for survival between the primary nuclei and their initial ordering along the nanowire. Then, the surviving growing nanoclusters create "spatial shadow regions" around themselves, which add a new factor in the selection of clusters that determine the final ordering in a one-dimensional synthesized system. Note that in this case, atoms in the space surrounding these nanoclusters move chaotically and not directly towards their surfaces. Under such conditions, a nanocluster adsorbing free atoms creates a shadow in all directions, the effect of which, in contrast to a geometric shadow arising in a ballistic mode, weakens with distance from its surface. We have shown that the use of a time-dependent level of supply of free atoms to the system can minimize the "noise" in the periodicity of synthesized clusters by controlling the contributions of surface shadow and spatial shadow effects to the process of self-ordering.

A variety of forms of synthesized nanoclusters is achieved by changing the orientation of the nanowire axis relative to the internal crystal structure. The feature of the morphology of each synthesized structure is determined by the self-consistency of anisotropic diffusion fluxes (free atoms from the surrounding space and deposited atoms from adjacent sections of the nanowire) with the anisotropic distribution of surface energy density.

References

1. Chung, S., Yu, J. and Heath, J., 2000. Silicon nanowire devices. *Applied Physics Letters*, 76(15), pp.2068-2070.
2. Colli, A., Hofmann, S., Fasoli, A., Ferrari, A., Ducati, C., Dunin-Borkowski, R. and Robertson, J., 2006. Synthesis and optical properties of silicon nanowires grown by different methods. *Applied Physics A*, 85(3), pp.247-253.
3. Au, F., Wong, K., Tang, Y., Zhang, Y., Bello, I. and Lee, S., 1999. Electron field emission from silicon nanowires. *Applied Physics Letters*, 75(12), pp.1700-1702.
4. Holmes, J., Ziegler, K., Johnston, K., Doty, R. and Korgel, B., 1999. Artificial Atoms of Silicon. *MRS Proceedings*, 582.
5. Ding, S., Ikeda, M., Fukuda, M., Miyazaki, S. and Hirose, M., 1998. Quantum confinement effect in self-assembled, nanometer silicon dots. *Applied Physics Letters*, 73(26), pp.3881-3883.
6. Marsen, B. and Sattler, K., 1999. Fullerene-structured nanowires of silicon. *Physical Review B*, 60(16), pp.11593-11600.
7. Goldberger, J., Hochbaum, A., Fan, R. and Yang, P., 2006. Silicon Vertically Integrated Nanowire Field Effect Transistors. *Nano Letters*, 6(5), pp.973-977.
8. Zhong, Z., Fang, Y., Lu, W. and Lieber, C., 2005. Coherent Single Charge Transport in Molecular-Scale Silicon Nanowires. *Nano Letters*, 5(6), pp.1143-1146.
9. Demami, F., Ni, L., Rogel, R., Salaun, A. and Pichon, L., 2010. Silicon nanowires synthesis for chemical sensor applications. *Procedia Engineering*, 5, pp.351-354.
10. Cui, Y., 2001. Nanowire Nanosensors for Highly Sensitive and Selective Detection of Biological and Chemical Species. *Science*, 293(5533), pp.1289-1292.
11. Lechuga, L. et al, 2006. A highly sensitive microsystem based on nanomechanical biosensors for genomics applications. *Sensors and Actuators B: Chemical*, 118(1-2), pp.2-10.
12. Li, Z., Chen, Y., Li, X., Kamins, T., Nauka, K. and Williams, R., 2004. Sequence-Specific Label-Free DNA Sensors Based on Silicon Nanowires. *Nano Letters*, 4(2), pp.245-247.
13. Lobet, J., Rius, G., Chuquitarqui, A., Borrisé, X., Koops, R., van Veghel, M. and Perez-Murano, F., 2018. Arrays of suspended silicon nanowires defined by ion beam implantation: mechanical coupling and combination with CMOS technology. *Nanotechnology*, 29(15), p.155303.
14. Eom, K., Park, H., Yoon, D. and Kwon, T., 2011. Nanomechanical resonators and their applications in biological/chemical detection: Nanomechanics principles. *Physics Reports*, 503(4-5), pp.115-163.
15. Cui, Y., Wei Q., Park H. and Lieber C. M., 2001. Nanowire Nanosensors for Highly Sensitive and Selective Detection of Biological and Chemical Species. *Science*, 293(5533), pp.1289-1292.
16. Cui, H., Wang, B., Wang, W., Hao, Y., Liu, C., Song, K., Zhang, S. and Wang, S., 2018. Frosted Slides Decorated with Silica Nanowires for Detecting Circulating Tumor Cells

from Prostate Cancer Patients. *ACS Applied Materials & Interfaces*, 10(23), pp.19545-19553.
17. Legallais, M., Nguyen, T., Cazimajou, T., Mouis, M., Salem, B. and Ternon, C., 2019. Material engineering of percolating silicon nanowire networks for reliable and efficient electronic devices. *Materials Chemistry and Physics*, 238, p.121871.
18. Namdari, P., Daraee, H. and Eatemadi, A., 2016. Recent Advances in Silicon Nanowire Biosensors: Synthesis Methods, Properties, and Applications. *Nanoscale Research Letters*, 11(1).
19. Hochbaum, A., Fan, R., He, R. and Yang, P., 2005. Controlled Growth of Si Nanowire Arrays for Device Integration. *Nano Letters*, 5(3), pp.457-460.
20. Yang, C., Barrelet, C., Capasso, F. and Lieber, C., 2006. Single p-Type/Intrinsic/n-Type Silicon Nanowires as Nanoscale Avalanche Photodetectors. *Nano Letters*, 6(12), pp.2929-2934.
21. Vardi, A., Akopian, N., Bahir, G., Doyennette, L., Tchernycheva, M., Nevou, L., Julien, F., Guillot, F. and Monroy, E., 2006. Room temperature demonstration of GaN/AlN quantum dot intraband infrared photodetector at fiber-optics communication wavelength. *Applied Physics Letters*, 88(14), p.143101.
22. Dawood, M., Tripathy, S., Dolmanan, S., Ng, T., Tan, H. and Lam, J., 2012. Influence of catalytic gold and silver metal nanoparticles on structural, optical, and vibrational properties of silicon nanowires synthesized by metal-assisted chemical etching. *Journal of Applied Physics*, 112(7), p.073509.
23. Osminkina, L., Gonchar, K., Marshov, V., Bunkov, K., Petrov, D., Golovan, L., Talkenberg, F., Sivakov, V. and Timoshenko, V., 2012. Optical properties of silicon nanowire arrays formed by metal-assisted chemical etching: evidences for light localization effect. *Nanoscale Research Letters*, 7(1).
24. Stelzner, T., Pietsch, M., Andrä, G., Falk, F., Ose, E. and Christiansen, S., 2008. Silicon nanowire-based solar cells. *Nanotechnology*, 19(29), p.295203.
25. Sivakov, V., Andrä, G., Gawlik, A., Berger, A., Plentz, J., Falk, F. and Christiansen, S., 2009. Silicon Nanowire-Based Solar Cells on Glass: Synthesis, Optical Properties, and Cell Parameters. *Nano Letters*, 9(4), pp.1549-1554.
26. Law, M., Greene, L., Johnson, J., Saykally, R. and Yang, P., 2005. Nanowire dye-sensitized solar cells. *Nature Materials*, 4(6), pp.455-459.
27. Kempa, T. and Lieber, C., 2014. Semiconductor nanowire solar cells: synthetic advances and tunable properties. *Pure and Applied Chemistry*, 86(1), pp.13-26.
28. Tanabe, K., Fontcuberta i Morral, A., Atwater, H., Aiken, D. and Wanlass, M., 2006. Direct-bonded GaAs/InGaAs tandem solar cell. *Applied Physics Letters*, 89(10), p.102106.
29. Misra, S., Yu, L., Foldyna, M. and Roca i Cabarrocas, P., 2013. High efficiency and stable hydrogenated amorphous silicon radial junction solar cells built on VLS-grown silicon nanowires. *Solar Energy Materials and Solar Cells*, 118, pp.90-95.
30. Tang, J., Maurice, J., Chen, W., Misra, S., Foldyna, M., Johnson, E. and Roca i Cabarrocas, P., 2016. Plasma-Assisted Growth of Silicon Nanowires by Sn Catalyst: Step-by-Step Observation. *Nanoscale Research Letters*, 11(1).

31. Wallentin, J., Anttu, N., Asoli, D., Huffman, M., Aberg, I., Magnusson, M., Siefer, G., Fuss-Kailuweit, P., Dimroth, F., Witzigmann, B., Xu, H., Samuelson, L., Deppert, K. and Borgstrom, M., 2013. InP Nanowire Array Solar Cells Achieving 13.8% Efficiency by Exceeding the Ray Optics Limit. *Science*, 339(6123), pp.1057-1060.
32. Kempa, T., Day, R., Kim, S., Park, H. and Lieber, C., 2013. Semiconductor nanowires: a platform for exploring limits and concepts for nano-enabled solar cells. *Energy & Environmental Science*, 6(3), p.719.
33. Kim, S., Day, R., Cahoon, J., Kempa, T., Song, K., Park, H. and Lieber, C., 2012. Tuning Light Absorption in Core/Shell Silicon Nanowire Photovoltaic Devices through Morphological Design. *Nano Letters*, 12(9), pp.4971-4976.
34. Yu, X., Shen, X., Mu, X., Zhang, J., Sun, B., Zeng, L., Yang, L., Wu, Y., He, H. and Yang, D., 2015. High Efficiency Organic/Silicon-Nanowire Hybrid Solar Cells: Significance of Strong Inversion Layer. *Scientific Reports*, 5(1).
35. Gouda, A., Allam, N. and Swillam, M., 2017. Efficient fabrication methodology of wide angle black silicon for energy harvesting applications. *RSC Advances*, 7(43), pp.26974-26982.
36. Tian, B., Zheng, X., Kempa, T., Fang, Y., Yu, N., Yu, G., Huang, J. and Lieber, C., 2007. Coaxial silicon nanowires as solar cells and nanoelectronic power sources. *Nature*, 449(7164), pp.885-889.
37. Yu, X., Shen, X., Mu, X., Zhang, J., Sun, B., Zeng, L., Yang, L., Wu, Y., He, H. and Yang, D., 2015. High Efficiency Organic/Silicon-Nanowire Hybrid Solar Cells: Significance of Strong Inversion Layer. *Scientific Reports*, 5(1).
38. Day, R., Mankin, M., Gao, R., No, Y., Kim, S., Bell, D., Park, H. and Lieber, C., 2015. Plateau–Rayleigh crystal growth of periodic shells on one-dimensional substrates. *Nature Nanotechnology*, 10(4), pp.345-352.
39. Day, R., Mankin, M. and Lieber, C., 2016. Plateau–Rayleigh Crystal Growth of Nanowire Heterostructures: Strain-Modified Surface Chemistry and Morphological Control in One, Two, and Three Dimensions. *Nano Letters*, 16(4), pp.2830-2836.
40. Lauhon, L., Gudiksen, M., Wang, D. and Lieber, C., 2002. Epitaxial core–shell and core–multishell nanowire heterostructures. *Nature*, 420(6911), pp.57-61.
41. Mata, M., Zhou, X., Furtmayr, F., Teubert, J., Gradečak, S., Eickhoff, M., Fontcuberta i Morral, A. and Arbiol, J., 2013. A review of MBE grown 0D, 1D and 2D quantum structures in a nanowire. *Journal of Materials Chemistry C*, 1(28), p.4300.
42. Hochbaum, A., Chen, R., Delgado, R., Liang, W., Garnett, E., Najarian, M., Majumdar, A. and Yang, P., 2008. Enhanced thermoelectric performance of rough silicon nanowires. *Nature*, 451(7175), pp.163-167.
43. Lim, S., Crawford, S., Haberfehlner, G. and Gradečak, S., 2012. Controlled Modulation of Diameter and Composition along Individual III–V Nitride Nanowires. *Nano Letters*, 13(2), pp.331-336.
44. Hochbaum, A., Fan, R., He, R. and Yang, P., 2005. Controlled Growth of Si Nanowire Arrays for Device Integration. *Nano Letters*, 5(3), pp.457-460.
45. Takasaki, M., Tago, M., Oaki, Y. and Imai, H., 2020. Thermally induced fragmentation of nanoscale calcite. *RSC Advances*, 10(10), pp.6088-6091.

46. Zhang, Y., Yan, Y. and Zhu, F., 2007. The Periodic Instability of Diameter of ZnO Nanowires via a Self-oscillatory Mechanism. *Nanoscale Research Letters*, 2(10), pp.492-495.
47. Xue, Z., Xu, M., Zhao, Y., Wang, J., Jiang, X., Yu, L., Wang, J., Xu, J., Shi, Y., Chen, K. and Roca i Cabarrocas, P., 2016. Engineering island-chain silicon nanowires via a droplet mediated Plateau-Rayleigh transformation. Nature Communications, 7(1).
48. Biswas, S., Doherty, J., Majumdar, D., Ghoshal, T., Rahme, K., Conroy, M., Singha, A., Morris, M. and Holmes, J., 2015. Diameter-Controlled Germanium Nanowires with Lamellar Twinning and Polytypes. *Chemistry of Materials*, 27(9), pp.3408-3416.
49. Xue, Z., Xu, M., Li, X., Wang, J., Jiang, X., Wei, X., Yu, L., Chen, Q., Wang, J., Xu, J., Shi, Y., Chen, K. and Roca i Cabarrocas, P., 2016. In-Plane Self-Turning and Twin Dynamics Renders Large Stretchability to Mono-Like Zigzag Silicon Nanowire Springs. *Advanced Functional Materials*, 26(29), pp.5352-5359.
50. Hwang, S., Lee, C., Cheng, H., Jeong, J., Kang, S., Kim, J., Shin, J., Yang, J., Liu, Z., Ameer, G., Huang, Y. and Rogers, J., 2015. Biodegradable Elastomers and Silicon Nanomembranes/Nanoribbons for Stretchable, Transient Electronics, and Biosensors. *Nano Letters*, 15(5), pp.2801-2808.
51. Heiss, M., Fontana, Y., Gustafsson, A., Wüst, G., Magen, C., O'Regan, D., Luo, J., Ketterer, B., Conesa-Boj, S., Kuhlmann, A., Houel, J., Russo-Averchi, E., Morante, J., Cantoni, M., Marzari, N., Arbiol, J., Zunger, A., Warburton, R. and Fontcuberta i Morral, A., 2013. Self-assembled quantum dots in a nanowire system for quantum photonics. *Nature Materials*, 12(5), pp.439-444.
52. Panciera, F., Chou, Y., Reuter, M., Zakharov, D., Stach, E., Hofmann, S. and Ross, F., 2015. Synthesis of nanostructures in nanowires using sequential catalyst reactions. *Nature Materials*, 14(8), pp.820-825.
53. Haiguang M., Rongrong Y., Junzhuan W., Yi S., Jun X., Kunji C., and Linwei Y., 2020. Cylindrical Line-Feeding Growth of Free-Standing Silicon Nanohelices as Elastic Springs and Resonators. *Nano Lett.*, 20(7), pp.5072–5080
54. Gorshkov, V., Tereshchuk, V. and Sareh, P., 2019. Restructuring and breakup of nanowires with the diamond cubic crystal structure into nanoparticles. *Materials Today Communications*, p.100727.
55. Kamins, T., Li, X., Williams, R., 2003. Thermal stability of Ti-catalyzed Si nanowires, *Appl. Phys. Lett*., 82 (2), pp. 263–265.
56. Wen-Liang, L., Kai-Wang, Z., Jian-Xin, Z., 2009. Thermal stability of silicon nanowires: atomistic simulation study, *Chinese Phys. B*, 18(7), pp. 2920–2924.
57. Kuech, T., Nishinaga, T., 2015. *Handbook Of Crystal Growth*. Amsterdam: Elsevier.
58. Evans, J.W., Thiel, P.A., Bartelt, M.C., 2006. Morphological evolution during epitaxial thin film growth: Formation of 2D islands and 3D mounds, *Surface Science Reports*, 61 (1–2), pp.1-128.
59. Gorshkov, V., Zavalov, A., and Privman, V., 2009. Shape Selection in Diffusive Growth of Colloids and Nanoparticles, *Langmuir*, 25, pp.7940–7953.
60. Gorshkov, V. and Privman, V., 2010. Models of Synthesis of Uniform Colloids and Nanocrystals, *Physica E*, 43, pp. 1–12.

61. Privman, V., Gorshkov, V., and Yaish, Y. E., 2017. Kinetics Modeling of Nanoparticle Growth on and Evaporation off Nanotubes, *J. Appl. Phys*., 121, 014301-1–014301-8.
62. Gorshkov, V., Kuzmenko, V., and Privman, V., 2014. Nonequilibrium Kinetic Modeling of Sintering of a Layer of Dispersed Nanocrystals, *CrystEngComm*, 16, pp. 10395–10409.
63. Gorshkov, V., Kuzmenko, V., and Privman, V., 2014. Modeling of Growth Morphology of Core–Shell Nanoparticles. *The Journal of Physical Chemistry C* 118, pp. 24959-24966.
64. Privman, V., Gorshkov, V., and Zavalov, O., 2014. Formation of Nanoclusters and Nanopillars in Nonequilibrium Surface Growth for Catalysis Applications: Growth by Diffusional Transport of Matter in Solution Synthesis, *Heat Mass Transfer*, 50, pp. 383–392.
65. Gorshkov, V., Zavalov, O., Atanassov, P. B., and Privman, V., 2010. Morphology of Nanoclusters and Nanopillars Formed in Nonequilibrium Surface Growth for Catalysis Applications, *Langmuir*, 27, pp. 8554–8561.
66. Gorshkov, V., Sareh, P., Tereshchuk, V., Soleiman- Fallah, A., 2019. Dynamics of Anisotropic Break- Up in Nanowires of FCC Lattice Structure. *Advanced Theory and Simulations*, pp.1900118.
67. Gorshkov, V. and Privman, V., 2017. Kinetic Monte Carlo model of breakup of nanowires into chains of nanoparticles. *Journal of Applied Physics*, 122(20), p.204301.
68. Gorshkov, V., Tereshchuk, V. and Sareh, P., 2019. Restructuring and breakup of nanowires with the diamond cubic crystal structure into nanoparticles. *Materials Today Communications*, p.100727.
69. Gorshkov, V., Tereshchuk, V. and Sareh, P., 2020. Diversity of anisotropy effects in the breakup of metallic FCC nanowires into ordered nanodroplet chains. *CrystEngComm*, 22(15), pp.2601-2611.
70. Eaglesham, D., White, A., Feldman, L., Moriya, N., Jacobson, D., 1993. Equilibrium shape of Si, *Phys. Rev. Lett*. 70 (11), pp.1643–1646.
71. Wang, C. M., Baer, D. R., Amonette, J. E., Engelhard, M. H., Qiang, Y. and Antony, J., 2007. Morphology and oxide shell structure of iron nanoparticles grown by sputter-gas-aggregation. *Nanotechnology* 18, 255603.
72. Heyraud, J., Métois, J., Bermond, J., 1999. The roughening transition of the Si{113} and Si {110} surfaces – an in situ, real time observation. *Surf. Sci*., 425 (1), pp. 48–56.
73. Suzuki, T., Minoda, H., Tanishiro, Y., Yagi, K., 1999. REM studies of the roughening transitions of Si high index surfaces, *Thin Solid Films* 343-344, pp. 423–426.
74. Liu, H. and Dandy, D., 1996. *Diamond Chemical Vapor Deposition*. Estados Unidos: Noyes Publications.
75. Ye, H. and Yu, J., 2014. Germanium epitaxy on silicon. *Science and Technology of Advanced Materials*, 15(2), p.024601.
76. Sibirev, N., Tchernycheva, M., Timofeeva, M., Harmand, J., Cirlin, G. and Dubrovskii, V., 2012. Influence of shadow effect on the growth and shape of InAs nanowires. *Journal of Applied Physics*, 111(10), p.104317.
77. Barranco, A., Borras, A., A. Gonzalez-Elipe, R., Palmero, A., 2016. Perspectives on oblique angle deposition of thin films: From fundamentals to devices. *Progress in Materials Science*, 76, pp. 59–153.

Supplementary Materials

Heterogeneous and homogeneous nucleation in the synthesis of quasi-one-dimensional periodic core-shell nanostructures

Vyacheslav N. Gorshkov[1], Vladimir V. Tereshchuk[1]

[1] National Technical University of Ukraine, Igor Sikorsky Kyiv Polytechnic Institute, 37 Prospect Peremogy, Kiev 03056, Ukraine.

1. **Synthesis of second generation nanoclusters**. Large nanoclusters that have been grown during the synthesis largely suppress the possibility of generating second-generation nanodroplets in the intervals between them. First, the fluxes of free atoms to the basic nanowire in these gaps are weakened due to the shadow effect created by large clusters. Second, the surface diffusion of deposited atoms that nevertheless reached the surface of the nanowire leads to the absorption of these atoms by primary clusters. However, the "populating" of intermediate zones becomes possible if the supply of free atoms to the system is increased. Naturally, the level of supply (the value of the parameter β) determines the number of secondary nanoclusters according to the same laws that establish the principles of self-organization at the first stage of synthesis. Results of our simulations presented in Fig. S1 demonstrate the discussed effects, which were observed in experiments [39]. At the initial/preparatory stage, nanoclusters are grown at large distance from each other to reduce the shadow effects. Subsequent population of intercluster gaps can be realized both with a different number of secondary nanodroplets and with different surface morphology, depending on the value of the parameter β. Note that in all the variants presented, the shadow effects from the large clusters are up to some extent inescapable.

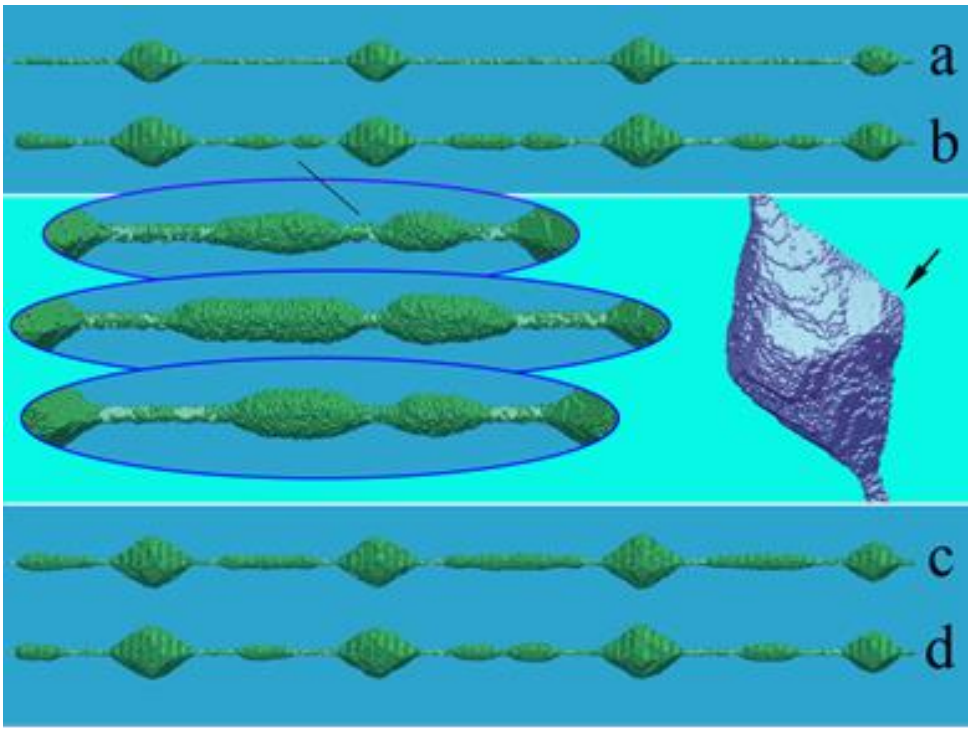

Figure S1. The results of two-stage synthesis process of nanoclusters. Subimage (a) depicts the synthesized structure at the end of the first stage ($t_1 = 3.77 \times 10^7$ MC steps). Cold regime, [100]-orientation: $\alpha = 3, p = 0.32$, $L = 900$, $d = 4$, $\beta = 1.075$. (a) - $t = 3.77 \times 10^7$ MC steps, $N_a = 396 \times 10^3$. Subimages (b), (c), (d) show the shapes of the nanowire at the second stage of synthesis with the increased parameter $\beta(t > t_1) = 1.2, 1.25$ and 1.18, respectively. These configurations correspond to the time moments $t = 4.4, 4.3$ and 4.55×10^7 MC steps. Insets depict enlarged structures of the populated intervals for subimage (b) and the shape of one of the large clusters.

2. Shadow effect in the nanoclusters ordering. The role of this phenomenon in self-organization processes is manifested at intermediate stages of synthesis, when rather large primary clusters have already been formed as a result of surface diffusion. The outermost clusters synthesized by the time $t = t_5$ (see Fig. S2) create near themselves zones of low surface concentration of deposited atoms ("diffusive" regions). However, under these conditions, the formation of new (delayed) nuclei in areas of low overlap of neighboring "diffusive" regions is

not excluded – see in Fig. S2 dynamics of such a nanocluster that is enclosed by the olive ellipse ($t_5 \le t \le t_{11}$). Its gradual disappearing ($t > t_{11}$) is the result that the growing left/right neighbors screen spatial diffusive fluxes that "feed" this delayed nucleus. One can see that the dissolving cluster slightly drifts to the right because of the a symmetrical screening of these fluxes by the different in size having grown primary clusters.

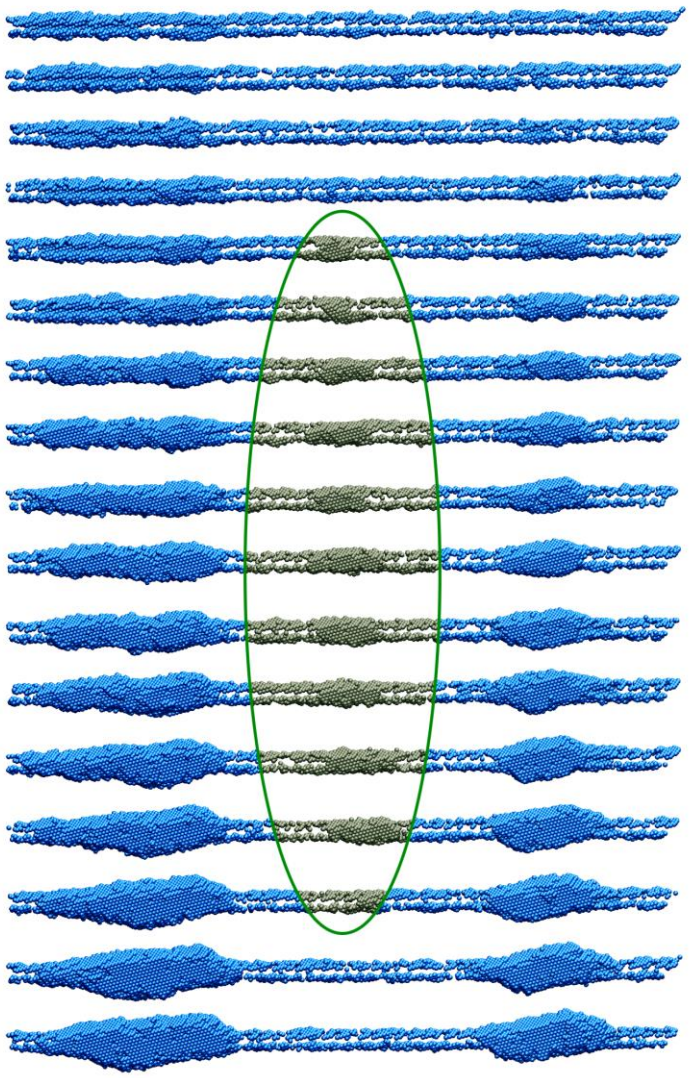

Figure S2. The shadow effect in the dynamics of the nanoclusters synthesized. Fragments of a long nanowire are depicted at the time moments $t_i = [2 + 0.2 \times (i-1)] \times 10^6$ MC steps, $i = 1, 2, 3, \ldots, 17$ (from up to down) Warm regime: $\alpha = 2.7$, $p = 0.36$, $d = 4$, $\beta = 2.6$; The nanowire is oriented along the bisector-direction, the length of fragments is $l_{frag} = 225$.

3. Influence of the state of the basic nanowire surface on the formation of synthesized nanostructures. In the main text, it is shown that the characteristic distance between the formed nuclei, l_{inr}, is directly proportional to the surface diffusion coefficient of atoms, D_s - see Eq. (9). In our numerical experiments, we varied the D_s value by changing the rules for the formation of the basic nanowire. In most cases, it consisted of occupied cells of the crystal lattice, which are located inside a straight cylinder of length L and radius r_0. Results presented in Fig. S3 are obtained for the case when the radius of the nanowire is determined randomly for each candidate cell: $r = r_0 + \varepsilon \times (1 - 2\eta)$, where η is a random number, $\eta \in [0,1]$. Thus, the surface of the nanowire took the form of an acicular/rough structure, which reduces the surface diffusion fluxes of hopping deposited atoms. As a result, the distance between the primary nuclei is significantly reduced and the synthesized nanoclusters have a rather elongated shape, which sharply differs from the nanoclusters formed on a smooth nanowire (see Fig. 7 in the main text).

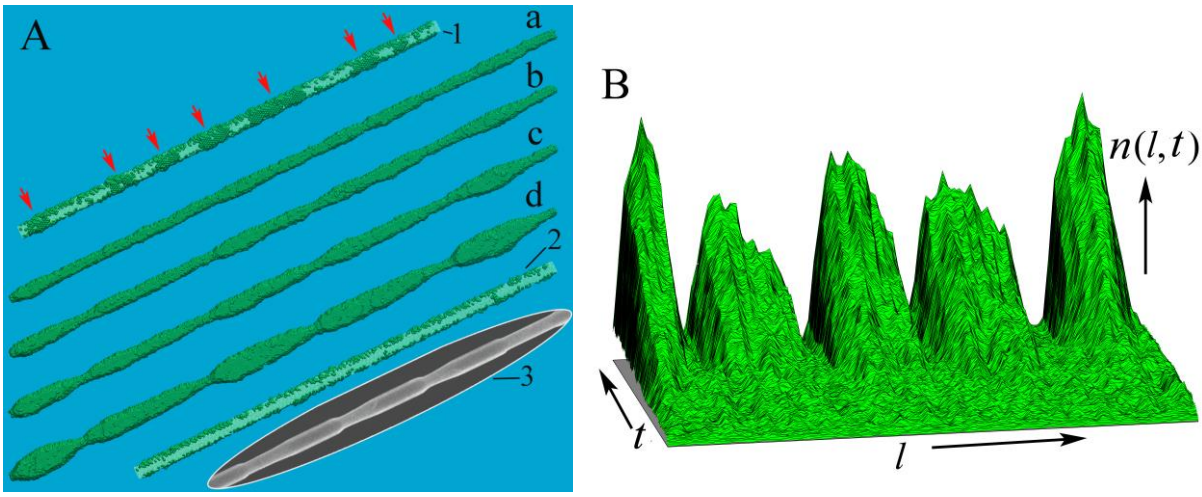

Figure S3. Synthesis of periodic shells on nanowires with [112] orientation and sharpened surface of the basic nanowire - $r_0 = 2.3$. Warm regime: $\alpha = 2.7, p = 0.36$, $L = 480$, $\beta = 2.4$ (A) Subimages from (a) to (d) depict shape of the synthesized structure at $t = 4, 5, 6, 8 (\times 10^6)$ MC steps, $N_t \approx 127 \times 10^3$. Insets (1) and (2) are snapshots of the nanowire fragments with length $\hat{L} = 200$, at $t = 0.8 \times 10^6$ when the surface is rough and smooth ($\varepsilon = 0$), respectively. Inset (3) presents one of the experimental results obtained in [38]. (B) The dynamics of the linear density of adsorbed atoms, $n(l,t)$, for the nanowire shown in subpart (A).

4. Synthesis of nonsymmetrical nanoclusters. If the orientation of the nanowire does not coincide with one of the axes of symmetry of Wulff construction then the shape of synthesized clusters can be non symmetrical too - See Fig. S4.

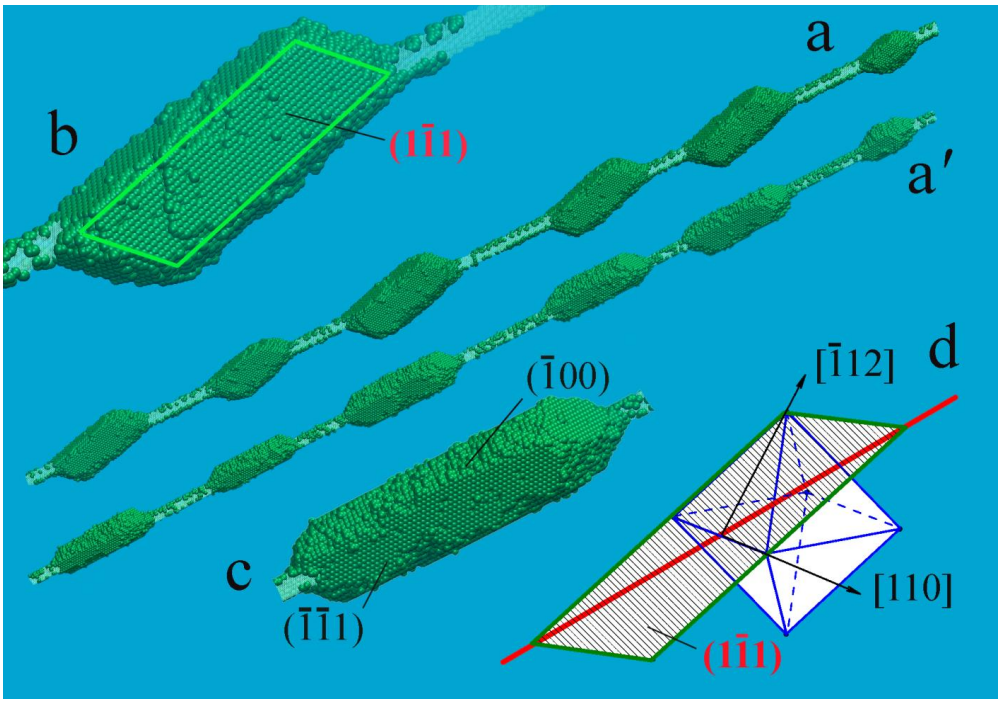

Figure S4. Synthesis of periodic nanostructures on the nanowire with bisector-orientation in case of exponential decreasing the parameter β: $\beta = 2.5 + 0.3 \times \exp\left(-\frac{t}{1.9\times10^6}\right)$. Warm regime: $\alpha = 2.7, p = 0.36,\ L = 400,\ d = 4$. Subimages (a) and (a') depict a side and top view of the nanowire. Subimages (b) and (c) show the views of a single synthesized nanocluster. Subimage (d) present the nanowire orientation (red line) relative to the "main" facets [111]-type that build the Wulff construction. $t = 8.6 \times 10^6$ MC steps, $N_t \approx 79.3 \times 10^3$.